Hybrid RIS-Assisted MIMO Dual-Function Radar-Communication System

Zhuoyang Liu, *Graduate Student Member, IEEE*, Haiyang Zhang, *Member, IEEE*, Tianyao Huang, *Member, IEEE*, Feng Xu, *Senior Member, IEEE*, and Yonina C. Eldar, *Fellow, IEEE*

***Abstract*—Dual-function radar-communication (DFRC) technology is emerging in next-generation wireless systems. Reconfigurable intelligent surface (RIS) arrays have been suggested as a crucial sensor component of the DFRC. In this paper, we propose a hybrid RIS (HRIS)-assisted multiple-input multiple-output (MIMO) DFRC system, where the HRIS is capable of reflecting communication signals to mobile users and receiving the scattering signal reflected from the radar target simultaneously. Under such a scenario, we are interested in characterizing the fundamental trade-off between radar sensing and communication. Specifically, we study the joint design of the beamforming vectors at the base station (BS) and the parameter configuration of the HRIS so as to maximize the signal-to-interference-and-noise ratio (SINR) of the radar while guaranteeing a communication SINR requirement. To solve the formulated non-convex beamforming design problem, we propose an efficient alternating optimization (AO) approach. In particular, for fixed beams at the BS, we use a fast grid search-assisted auto gradient descent (FGS-AGD) algorithm to seek the best HRIS configuration; Then, a closed-form BS beamforming solution is obtained using semidefinite relaxation. Numerical results indicate that compared with benchmark schemes, the proposed approach is capable of improving the radar performance and communication quality significantly and simultaneously.**

***Index Terms*—Dual-function radar-communication, hybrid RIS, joint beamforming design, alternating optimization approach.**

I. Introduction

DUAL-FUNCTION radar-communication (DFRC) systems have attracted significant attention in wireless networks. They enable radar sensing and communication functionalities by sharing the same hardware platform [1]. DFRC systems have the potential to be applied in autonomous driving, virtual reality, and other control settings due to their integrating radar and communication properties [2]. To enable the coexistence of both radar and communication, numerous researchers have studied the implementation of DFRC in recent years. For example, the authors in [3] use the frequency and spatial agility properties of the carrier agile phased array radar to implement a DFRC and achieved comparable communication performance to an independent device while guaranteeing radar performance. In [4], the authors utilize frequency-hopping waveform codes to obtain different orthogonal radar waveforms and embed phase-shift keying to implement communication. Though DFRC technology has made significant progress, it still faces several challenges in practice. A DFRC system may suffer severe signal degradation when the user is sheltered by trees or buildings. In addition, when detecting short-range objects, the DFRC antennas need to operate in duplex mode to avoid signal coupling between the transmit and receive channels, which is difficult to implement in most practical base stations (BSs) [5].

Recently, reconfigurable intelligent surface (RIS) technology has emerged for future six-generation wireless systems. RIS is capable of enhancing communication performance by modifying the radio propagation, i.e., making the electromagnetic (EM) environment better for wireless communication [6], [7]. The passive reflection process of the RIS is similar to radar target scattering, which can be utilized to facilitate radar sensing by adjusting the reflection parameters of the RIS [8]. Consequently, RIS has also been introduced to the field of DFRC [9], [10], which enables broadening the communication field of view (FOV) and radar detection by generating desirable reflecting beam patterns [11]. However, the conventional RIS-assisted DFRC systems have two drawbacks. First, due to the passive reflection properties of the RIS, using RIS to achieve communication will bring signal fading [12] and make transmitter-RIS and RIS-receiver links cascaded that are difficult to measure separately [13]. For instance, RIS transforms the coherent superposition from a BS into an incoherent superposition of the BS transmitted signals and RIS reflected signals, and the original channel from BS to users into BS-RIS and RIS-user cascaded channel [14]. The second drawback of the passive RIS-assisted DFRC system is that one can only reflect the impinging signal and requires an additional radar receiver for radar echo acquisition.

Manuscript received 27 March 2023; revised 20 September 2023, 17 December 2023, and 21 February 2024; accepted 22 February 2024. Date of publication 28 February 2024; date of current version 3 April 2024. This work was supported by the National Natural Science Foundation of China under Grant 62231010 and in part by the Nanjing Overseas Students Science and Technology Innovation Project under Grant NJKCZYZZ2023-01. The associate editor coordinating the review of this manuscript and approving it for publication was Dr. Ali Tajer. *(Corresponding author: Feng Xu.)*

Zhuoyang Liu and Feng Xu are with the Key Lab for Information Science of Electromagnetic Wave (MoE), Fudan University, Shanghai 200433, China (e-mail: liuzy20@fudan.edu.cn; fengxu@fudan.edu.cn).

Haiyang Zhang is with the School of Communication and Information Engineering, Nanjing University of Posts and Telecommunications, Nanjing 210003, China (e-mail: haiyang.zhang@njupt.edu.cn).

Tianyao Huang is with the School of Computer and Communication Engineering, University of Science and Technology Beijing, Beijing 100083, China (e-mail: huangtianyao@ustb.edu.cn).

Yonina C. Eldar is with the Faculty of Mathematics and Computer Science, Weizmann Institute of Science, Rehovot 7610001, Israel (e-mail: yonina.eldar@weizmann.ac.il).

Digital Object Identifier 10.1109/TSP.2024.3371193

To overcome the aforementioned challenges with conventional RIS systems, hybrid RISs (HRISs) have been suggested, that combine RISs with dynamic metasurface antennas (DMAs) to provide a particular amount of energy to each reflection unit on the intelligent surface for signal reception [15]. In contrast to conventional RIS-assisted systems, the HRIS contains a few radio frequency (RF) connections to receive incoming signals while keeping the passive reflection performance of the meta-material elements. Recognizing the presence of various HRISs, including the simultaneously transmitting and reflecting (STAR)-RIS discussed in [16], [17], [18], the Multi-Functional RIS (MF-RIS) referenced in [19], and the semi-passive RIS applied in [16], our system stands out due to its additional reception functionality. In our system, each element possesses the unique ability to both reflect and receive the incoming signal concurrently, setting it apart from existing HRIS configurations. For convenience, we adopt the abbreviation 'HRIS' to represent our proposed HRIS configuration in the subsequent sections. An HRIS-assisted system can employ HRIS's signals or combine HRIS and BS signals for signal processing in order to perform radar detection, sensing, positioning, and communication integration. Based on this incorporation of reflection and reception functionalities, HRISs have potential applications in individual channel estimation [20] and near-field user localization problems [21]. Moreover, their potential to simultaneously enhance the performance of radar detection and user communication deserves exploring. This motivates the study of using the HRIS as an efficient means of facilitating radar detection and user communication.

In this paper, we consider an HRIS-assisted multiple-input multiple-output (MIMO) DFRC system, where the HRIS not only reflects the signal from the BS to both the radar targets and communication users but also receives the echoes from the targets. The proposed HRIS-assisted MIMO DFRC system comprises a BS and a HRIS and the control center, which utilizes both BS and HRIS devices for sensing and communication. Based on the above architecture, the control center configures the transmitted signals of the BS, and modifies the reflecting signal and receiving signal of the HRIS to implement passing communication symbols to users and radar targets scattering echo reception. Compared with conventional MIMO DFRC, the proposed system obtains improvements in both the radar and communication parts. Specifically, the presented DFRC system broadens the view of communication and assists the communication with non-line of sight users [7], [22]. On the other hand, the radar receiver is embedded in the HRIS, usually located remotely from the BS, which does not require the BS to work in full-duplex mode [15], [20]. Moreover, the HRIS is comprised of cheap meta-material elements and has low hardware complexity, which makes the HRIS-assisted MIMO DFRC system more portable and deployable [23].

To the best of our knowledge, we are the first to propose an HRIS-assisted MIMO DFRC system, which utilizes the unique capabilities of the HRIS to enhance both radar and communication performance simultaneously. Differing from the existing STAR-RIS systems, the proposed system leverages the HRIS to reflect the downlink communication signal to the user and receive the radar echo for sensing. Under such an HRIS-assisted MIMO DFRC system, our focus lies in the joint beamforming design at the HRIS and BS to achieve a balanced performance for both radar and communications. We formulate a comprehensive mathematical model for the HRIS-assisted MIMO DFRC system. Our model incorporates both the joint transmit beam signal processing carried out by the BS, as well as the reflection and reception configuration designs of the HRIS. Subsequently, a multi-parameter optimization problem corresponding to the joint beamforming of the HRIS-assisted MIMO DFRC system is formulated.

Specifically, we jointly design the transmit beamforming vectors at the BS and the configurations of HRIS to maximize the radar performance while guaranteeing communication performance. However, the joint beamforming design is a multi-parameter and combinatorial optimization problem, which is non-convex and, consequently, challenging to solve. To address this, we propose an alternating method to solve the resulting problem by recasting the original problem into two sub-problems: the HRIS configuration design and the design of the radar and communication transmitted beam of the BS. For the solution of these sub-problems, we suggest an alternating optimization (AO) approach to design the parameters of the HRIS configuration and BS's beamforming vectors. In particular, a gradient descent-based algorithm is proposed for the HRIS configuration design, and a semidefinite relaxation (SDR) technique with bisection search is applied for BS beamforming optimization. However, due to the high complexity of the HRIS configuration, we proposed a fast grid search (FGS) assisted auto gradient descent (AGD) algorithm that combines the efficiency of fast grid search with the flexibility of PyTorch auto-differentiation (AD). This approach is specifically designed to overcome the challenges of optimizing large HRIS configurations.

Extensive numerical results show that the performance of both radar and communication of HRIS-assisted DFRC outperforms the BSs-only and random-configured HRIS systems. Furthermore, we study the impact of the integrated beampattern and power allocation of the HRIS and the BSs on radar detection and wireless communication. In particular, under the same communication threshold and transmitted power, we show that the proposed system achieves a remarkable 3 dB improvement in radar performance compared to the BSs-only system and an impressive 6 dB gain over the random-configured HRIS system.

The rest of this paper is organized as follows: Section II presents the HRIS-assisted MIMO DFRC system, reviews the considered antenna architectures, and formulates the joint optimization problem in our DFRC system. Section III presents efficient methods to optimize the beampattern in both antenna architectures of the BS and HRIS, while Section IV numerically demonstrates the solution of this proposed system and evaluates its performance in different DFRC settings. Finally, Section V concludes the paper.

Throughout the paper, we use boldface lower-case and upper-case letters for vectors and matrices, respectively. For a matrix $\boldsymbol{A}$, the (i,j)-th element of $\boldsymbol{A}$ is denoted by $[\boldsymbol{A}]_{i,j}$. The ℓ_2 norm, conjugate operation, transpose, Hermitian transpose, element-wise product, and stochastic expectation are written as $|\cdot|^2$, $(\cdot)^*$, $(\cdot)^T$, $(\cdot)^H$, $\odot$, and $\mathbf{E}(\cdot)$, respectively. We use $\boldsymbol{I}_N$ to denote

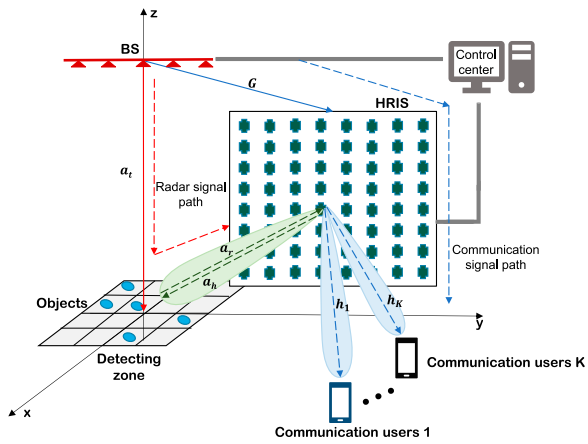

Fig. 1. The geometry of detecting zone and user terminals.

an N-dimensional identity matrix, $\mathbf{0}_{M\times N}$ is an $M \times N$ zero matrix, and $\mathbb{C}$ is the complex set.

II. System Model and Problem Formulation

In this section, we first present the general system model of the proposed HRIS-assisted MIMO DFRC system in Section II-A. We describe HRIS operation in Section II-B. Then, we introduce the performance evaluation metrics of radar and communication functionalities in such a DFRC system in Section II-C. Finally, we formulate the joint beamforming design problem in Section II-D.

A. System Model

We consider an HRIS-assisted MIMO DFRC system consisting of a BS, an HRIS, detecting zone and communication user terminals. We assume the BS consists of a uniform linear array (ULA) with T antennas, and the HRIS consists of N elements. In this system, both the BS and a HRIS are connected to a data control center by cables and controlled by the control center. This setup is graphically presented in Fig. 1, and it incorporates the downlink communication and radar object detection with the assistance of an HRIS. Specifically, the BS sends both radar signals and communication signals to perform radar detection and communication simultaneously. As in [20], we assume there is no direct link between the BS and communication users. The HRIS helps forward the communication signals to the communication users and receive the radar signals reflected from the detecting zone. In the case of multiple users, there are K communication users who receive the communicated signals from the reflection of the HRIS to communicate with the BS independently. For radar detection, the detecting zone in the HRIS system is the region where radar targets are located. The configuration of the detecting zone is determined by the antenna architecture of the BSs. To be specific, we divide the detecting zone into P rows and Q columns with the grid size being the field of view corresponding to the angle resolution of the BSs. Each block in the detecting zone can scatter the signal from both the BS and the HRIS, and the scattering signal is received by an RF chain on the HRIS.

We begin with the signals transmitted from the BS. The discrete-time joint transmit beam signal of the BS in time step n is written as

$$\boldsymbol{x}(n) = \boldsymbol{W_c}\boldsymbol{c}(n) + \boldsymbol{w}_r s(n), \tag{1}$$

where $\boldsymbol{c}(n) = [c_1(n), ..., c_K(n)]^T$ represents K communication symbol streams intended for K communication users, and $\boldsymbol{W}_c = [\boldsymbol{w}_1, ..., \boldsymbol{w}_K] \in \mathbb{C}^{T\times K}$ denotes the communication precoder matrix. Similarly, $s(n)$ is an individual radar waveform with unit power, and $\boldsymbol{w}_r \in \mathbb{C}^{T\times 1}$ is the controllable radar beamforming vector of T antennas. Without loss of generality, we assume each entry of the communication signals $\boldsymbol{c}(n)$ is a wide-sense stationary random process with zero-mean and unit power, and uncorrelated with each other, namely $\mathbf{E}(\boldsymbol{c}(n)\boldsymbol{c}^H(n)) = \boldsymbol{I}_K$. In addition, the communication symbols are uncorrelated with the radar waveform, meaning $\mathbf{E}(\boldsymbol{c}(n)s(n)) = \mathbf{0}_{K\times 1}$.

To illustrate the power constraint for the BS, we denote the covariance matrix of the transmitted beamforming matrix by $\boldsymbol{R} \triangleq \boldsymbol{W}\boldsymbol{W}^H$, where $\boldsymbol{W} = [\boldsymbol{W}_c, \boldsymbol{w}_r] \in \mathbb{C}^{T\times(K+1)}$ is the joint controllable matrix of the BS. Thus, each antenna's power constraint implies that

$$[\boldsymbol{R}]_{j,j} = [\boldsymbol{W}_c\boldsymbol{W}_c^H + \boldsymbol{w}_r\boldsymbol{w}_r^H]_{j,j} = P_t,\ j = 1, ..., T, \tag{2}$$

where P_t is the transmit power for each antenna.

B. Preliminaries of HRIS

HRIS is a new metamaterial device that achieves reflection and reception simultaneously. To achieve this hybrid operation, each metasurface element of the HRIS must be capable of reflecting a component of the impinging signal while also receiving another portion of it in a controlled manner [15]. The signals connected to the waveguides are then measured by the RF chain and utilized to determine radar and communication information. In [20], the authors presented such a hybrid metamaterial surface which was applied to reflect in a reconfigurable function while using the received component of the signal to recover the target's angle of arrival locally. Regarding the HRIS protocol, [24] entirely covers the configurations of hybrid meta-atoms, implementation methodologies, full-wave EM simulations, and its application in 6G wireless technology.

We model the coexistence of reflection and reception functions with a hybrid metasurface composed of N adjustable meta-atom elements. One straightforward approach to implement this operation is to link individual elements to waveguides. Subsequently, the signals arrived at these waveguides are received by the attached RF chain, which are then leveraged to extract essential information about radar sensing and communication. Meanwhile, these elements direct a portion of the impinging signal to the desired direction. As illustrated in Fig. 2, the control center can modify the reflected and received signals arriving at its surface by adjusting the surface's amplitude and phase shifts. Let $r_l(n)$ denote the discrete-time signal arriving at the l-th element of the HRIS in time

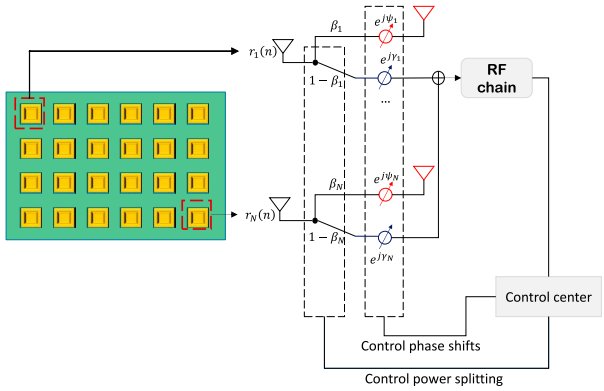

Fig. 2. The receiving and reflecting operation of the HRIS.

step n. Part of the signal is reflected to the desired direction with the adjustment by the parameter $\beta_l \in [0,1]$ and phase shift $\psi_l \in [0, 2\pi)$. The forward reflected signal is consequently given as

$$y_l^f(n) = \beta_l e^{j\psi_l} r_l(n),\ l = 1, ..., N. \tag{3}$$

Since per-element of the HRIS enables to locally receive signals via analog combining and digital processing, the received signal collected by the RF chain is expressed as

$$y_l^r(n) = (1-\beta_l) e^{j\gamma_l} r_l(n),\ l = 1, ..., N, \tag{4}$$

where $1-\beta_l$ is the amplitude allocated for receiving signal and $\gamma_l \in [0, 2\pi)$ is an additional phase shift that controls the phaser connected to the RF chain.

By concatenating the arrived signal $r_l(n)$ and reflected signal $y_l^f(n)$ from the whole HRIS into vectors $\boldsymbol{r}(n)$ and $\boldsymbol{y}^f(n)$, respectively, the received signal is formulated as

$$\boldsymbol{y}^f(n) = \boldsymbol{\Psi}(\boldsymbol{\beta}, \boldsymbol{\psi}) \boldsymbol{r}(n), \tag{5}$$

where the reflected matrix of the HRIS is defined as $\boldsymbol{\Psi}(\boldsymbol{\beta}, \boldsymbol{\psi}) = \text{diag}([\beta_1 e^{j\psi_1}, ..., \beta_N e^{j\psi_N}])$. Similarly, the reflected signal $y_l^r(n)$ from the RF chain can be concatenated as a vector $\boldsymbol{y}^r(n)$ given by

$$\boldsymbol{y}^r(n) = \boldsymbol{\phi}^H(\boldsymbol{\beta}, \boldsymbol{\gamma}) \boldsymbol{r}(n), \tag{6}$$

where the l-th element of the received vector is $[\boldsymbol{\phi}]_l = (1-\beta_l) e^{j\gamma_l}$.

The HRIS enables to change the EM environment by externally controllable parameters. The beampattern adjustment performance is dominated by amplitude distribution on the surface of the HRIS while slightly affected by the phased shifts in different elements of the HRIS [20]. Therefore, in this paper, we mainly control the beampattern of HRIS by adjusting the power splitting factor $\boldsymbol{\beta}$ with fixed phase shifts $\boldsymbol{\psi}$ and $\boldsymbol{\gamma}$. To be concrete, we optimize $\boldsymbol{\beta}$ with both $\boldsymbol{\psi}$ and $\boldsymbol{\gamma}$ set to zero in order to investigate the effect of power allocation on the HRIS-assisted MIMO DFRC system performance.

C. Performance Metrics of Radar and Communication

The main purpose of the HRIS-assisted DFRC system design is to achieve maximum radar sensing performance while ensuring efficient downlink multiuser communication. To meet multiuser communication requirements, both the BS beamforming and HRIS configuration are tailored. For radar detection tasks, BS's transmitted beam and HRIS's receiving beam are specifically designed toward the target located within the detecting zone. These performance metrics of multiuser communication and radar detection are formulated in the subsequent sections.

1) The Evaluation Metric of Communication: Let $\boldsymbol{G} \in \mathbb{C}^{N\times T}$ and $\boldsymbol{h}_k \in \mathbb{C}^{N\times 1}$ represent the channel from BS to HRIS and the channel from the HRIS to the k-th user, respectively. The received communication signal at the k-th user, denoted by $u_k(n)$, can be written as

$$u_k(n) = \boldsymbol{h}_k^H \boldsymbol{\Psi}(\boldsymbol{\beta}) \boldsymbol{G} \boldsymbol{x}(n) + v_k(n), \tag{7}$$

where $v_k(n)$ is additive white Gaussian noise (AWGN) with covariance σ^2.

We assemble the communication channels from the HRIS to multiple users, which we assume to be known, in the complex matrix $\boldsymbol{H} \triangleq [\boldsymbol{h}_1, ..., \boldsymbol{h}_K]^H \in \mathbb{C}^{K\times N}$. The signal received at K users is represented as the $K \times 1$ vector $\boldsymbol{u}(n) \triangleq [u_1(n), ..., u_K(n)]^T$ and we collect the $v_k(n)$ into a $K \times 1$ vector $\boldsymbol{v}(n)$. Combining (1) and (7), we rewrite the received signal at K users into radar-to-users parts and inter-users parts, given by

$$\boldsymbol{u}(n) = \boldsymbol{H}\boldsymbol{\Psi}(\boldsymbol{\beta})\boldsymbol{G}\boldsymbol{W}_c \boldsymbol{c}(n) + \boldsymbol{H}\boldsymbol{\Psi}(\boldsymbol{\beta})\boldsymbol{G}\boldsymbol{w}_r s(n) + \boldsymbol{v}(n). \tag{8}$$

Let the cascaded communication channel $\boldsymbol{H}_e = [\hat{\boldsymbol{h}}_1, ..., \hat{\boldsymbol{h}}_K]^H \in \mathbb{C}^{K\times T}$ be denoted as

$$\boldsymbol{H}_e(\boldsymbol{\beta}) = \boldsymbol{H}\boldsymbol{\Psi}(\boldsymbol{\beta})\boldsymbol{G}. \tag{9}$$

Similar to [25], we use the signal-to-interference-and-noise ratio (SINR) to evaluate communication performance. The communication power of the k-th user is

$$\mathbf{E}\left(|[\boldsymbol{H}_e(\boldsymbol{\beta})\boldsymbol{W}_c]_{k,k} c_k(n)|^2\right) = [\boldsymbol{H}_e(\boldsymbol{\beta})\boldsymbol{W}_c \boldsymbol{W}_c^H \boldsymbol{H}_e^H(\boldsymbol{\beta})]_{k,k}. \tag{10}$$

The communication inter-user interference power is given by

$$\mathbf{E}\left(\sum_{i\neq k}^{K} |[\boldsymbol{H}_e(\boldsymbol{\beta})\boldsymbol{W}_c]_{k,i} c_k(n)|^2\right) = \sum_{i\neq k}^{K} \left[\boldsymbol{H}_e(\boldsymbol{\beta})\boldsymbol{W}_c \boldsymbol{W}_c^H \boldsymbol{H}_e^H(\boldsymbol{\beta})\right]_{k,i}. \tag{11}$$

The interference power between the communication signals and the radar signal is

$$\mathbf{E}\left(|[\boldsymbol{H}_e(\boldsymbol{\beta})\boldsymbol{w}_r]_{k,1} s(n)|^2\right) = [\boldsymbol{H}_e(\boldsymbol{\beta})\boldsymbol{w}_r \boldsymbol{w}_r^H \boldsymbol{H}_e^H(\boldsymbol{\beta})]_{k,1}. \tag{12}$$

$$\eta_c(\boldsymbol{w}_r, \boldsymbol{W}_c, \boldsymbol{\beta}; k) = \frac{[\boldsymbol{H}_e(\boldsymbol{\beta})\boldsymbol{W}_c \boldsymbol{W}_c^H \boldsymbol{H}_e^H(\boldsymbol{\beta})]_{k,k}}{\sum_{i\neq k}^{K} [\boldsymbol{H}_e(\boldsymbol{\beta})\boldsymbol{W}_c \boldsymbol{W}_c^H \boldsymbol{H}_e^H(\boldsymbol{\beta})]_{k,i} + [\boldsymbol{H}_e(\boldsymbol{\beta})\boldsymbol{w}_r \boldsymbol{w}_r^H \boldsymbol{H}_e^H(\boldsymbol{\beta})]_{k,1} + \sigma^2}. \tag{13}$$

Therefore, the SINR of the k-th user is expressed by (13).

For convenience, let each column of $\boldsymbol{W}$ which represents the controllable codes of the BS be denoted by $\boldsymbol{w}_i$. The covariance matrix $\boldsymbol{R}$ of the transmitted beamforming matrix $\boldsymbol{W}$ can then be rewritten as the sum of sub-covariance matrices $\boldsymbol{R}_i \triangleq \boldsymbol{w}_i \boldsymbol{w}_i^H$ of different codes:

$$\boldsymbol{R} = \sum_{i=1}^{K+1} \boldsymbol{w}_i \boldsymbol{w}_i^H = \sum_{i=1}^{K+1} \boldsymbol{R}_i, \tag{14}$$

where beamforming matrix $\boldsymbol{W}$ consists of K communication precoder vectors and one radar precoder vector. Combining with the definition of the k-th user's cascaded communication channel in (9) and substituting (14) into (13), the k-th user's SINR can be expressed as (15), with the constraint (14) and

$$\text{rank}(\boldsymbol{R}_i) = 1, \ i = 1, ..., K+1. \tag{16}$$

2) The Evaluation Metric of Radar Detection: For radar detection, the BS transmits the joint signals that illuminate both the detecting zone and the HRIS. Subsequently, the HRIS will reflect the incoming signal resulting from the BS, directing it back towards the detecting zone. Therefore, the receiving signal at the HRIS comprises two components.

The arriving signal from the BS to the radar target can be expressed as

$$y(n; p, q) = \boldsymbol{a}_t^H(p, q)\boldsymbol{x}(n), \tag{17}$$

where $\boldsymbol{a}_t(p, q) \in \mathbb{C}^{T\times 1}$ is the steering vector from the BS to the (p, q) block in the detecting zone. Combined with (7), the signal forwarded by the HRIS is

$$\boldsymbol{r}_e(n) = \boldsymbol{\Psi}(\boldsymbol{\beta})\boldsymbol{G}\boldsymbol{x}(n), \tag{18}$$

and the arriving signal from the HRIS can be written as

$$r_s(n; p, q) = \boldsymbol{a}_h^H(p, q)\boldsymbol{r}_e(n), \tag{19}$$

where $\boldsymbol{a}_h(p, q) \in \mathbb{C}^{N\times 1}$ is the steering vector from the HRIS to the (p, q) block. Using the HRIS to receive the scattering signal and perform radar detection, the received signal at the HRIS can be consequently formulated as

$$\boldsymbol{r}(n; p, q) = \boldsymbol{\phi}^H(\boldsymbol{\beta})\boldsymbol{a}_r(p, q)(r_s(n; p, q) + y(n; p, q)), \tag{20}$$

where $\boldsymbol{a}_r(p, q) \in \mathbb{C}^{N\times 1}$ is the steering vector from the (p, q) block in the detecting zone to the n-th element on the HRIS.

For convenience of the analysis, we define the cascaded reflected vector $\hat{\boldsymbol{a}}_h \in \mathbb{C}^{T\times 1}$ and the cascaded received scalar A_r as

$$\begin{aligned} \hat{\boldsymbol{a}}_h^H(\boldsymbol{\beta}) &= \boldsymbol{a}_h^H(p, q)\boldsymbol{\Psi}(\boldsymbol{\beta})\boldsymbol{G}, \\ A_r(\boldsymbol{\beta}) &= \boldsymbol{\phi}^H(\boldsymbol{\beta})\boldsymbol{a}_r(p, q). \end{aligned} \tag{21}$$

Similar to the work in [26], we use the SINR as the radar performance metric. To this end, we split the receiving signal at the RF chain of the HRIS into two components: the primary valid signal and the interference signal. In our considered HRIS-assisted DFRC system, the scattering signal that came from the illumination of the BS's transmitted waveform is assumed as the valid primary signal. Meanwhile, the scatter back resulting from the illumination of the HRIS's reflected beam is defined as interference. Then, by substituting the expressions of the reflected vector and received scalar into (20), the valid signal is $A_r(\boldsymbol{\beta})s(n)\boldsymbol{a}_t^H\boldsymbol{w}_r$. The useful radar sensing power of the (p, q) block is then derived as

$$\mathbf{E}\left(|A_r(\boldsymbol{\beta})s(n)\boldsymbol{a}_t^H\boldsymbol{w}_r|^2\right) = |A_r(\boldsymbol{\beta})|^2\boldsymbol{a}_t^H\boldsymbol{w}_r\boldsymbol{w}_r^H\boldsymbol{a}_t. \tag{22}$$

The interference power from HRIS to the (p, q) block is

$$\mathbf{E}\left(|A_r(\boldsymbol{\beta})\hat{\boldsymbol{a}}_h^H(\boldsymbol{\beta})\boldsymbol{x}(n)|^2\right) = |A_r(\boldsymbol{\beta})|^2\hat{\boldsymbol{a}}_h^H(\boldsymbol{\beta})\boldsymbol{W}\boldsymbol{W}^H\hat{\boldsymbol{a}}_h(\boldsymbol{\beta}). \tag{23}$$

Combining (22) with (23), the SINR of the radar is expressed as

$$\eta_r(\boldsymbol{W}, \boldsymbol{\beta}; p, q) = \frac{|A_r(\boldsymbol{\beta})|^2\boldsymbol{a}_t^H\boldsymbol{w}_r\boldsymbol{w}_r^H\boldsymbol{a}_t}{|A_r(\boldsymbol{\beta})|^2\hat{\boldsymbol{a}}_h^H(\boldsymbol{\beta})\boldsymbol{W}\boldsymbol{W}^H\hat{\boldsymbol{a}}_h(\boldsymbol{\beta}) + \sigma^2}. \tag{24}$$

Furthermore, taking into account the scattering signal from the user, the expression of the SINR for the radar is depicted as (25), where $\boldsymbol{\phi}^H\boldsymbol{H}^H\boldsymbol{H}_e(\boldsymbol{\beta})\boldsymbol{W}\boldsymbol{W}^H\boldsymbol{H}_e^H(\boldsymbol{\beta})\boldsymbol{H}\boldsymbol{\phi}$ is the interference power from the user scattering. Our goal is to establish a foundational understanding of the HRIS-assisted DFRC system, focusing on the radar's SINR without considering user scattering. In this work, we proceed to explore and evaluate the performance metric of radar via (24) in the following section.

Compared with other DFRC works [25], [26], we use the same metrics to evaluate radar and communication performance. However, due to the coexistence of the HRIS device and the BS in our proposed DFRC system, we have another parameter $\boldsymbol{\beta}$ that affects both radar and communication performance.

$$\eta_c(\boldsymbol{R}, \boldsymbol{R}_k, \boldsymbol{\beta}; k) = \frac{\hat{\boldsymbol{h}}_k^H(\boldsymbol{\beta})\boldsymbol{R}_k\hat{\boldsymbol{h}}_k(\boldsymbol{\beta})}{\hat{\boldsymbol{h}}_k^H(\boldsymbol{\beta})\boldsymbol{R}\hat{\boldsymbol{h}}_k(\boldsymbol{\beta}) - \hat{\boldsymbol{h}}_k^H(\boldsymbol{\beta})\boldsymbol{R}_k\hat{\boldsymbol{h}}_k(\boldsymbol{\beta}) + \sigma^2}, \ k = 1, ..., K. \tag{15}$$

$$\eta_r(\boldsymbol{W}, \boldsymbol{\beta}; p, q) = \frac{|A_r(\boldsymbol{\beta})|^2\boldsymbol{a}_t^H\boldsymbol{w}_r\boldsymbol{w}_r^H\boldsymbol{a}_t}{|A_r(\boldsymbol{\beta})|^2\hat{\boldsymbol{a}}_h^H(\boldsymbol{\beta})\boldsymbol{W}\boldsymbol{W}^H\hat{\boldsymbol{a}}_h(\boldsymbol{\beta}) + \boldsymbol{\phi}^H\boldsymbol{H}^H\boldsymbol{H}_e(\boldsymbol{\beta})\boldsymbol{W}\boldsymbol{W}^H\boldsymbol{H}_e^H(\boldsymbol{\beta})\boldsymbol{H}\boldsymbol{\phi} + \sigma^2}, \tag{25}$$

D. Problem Formulation

From (15) and (24), both the radar and communication performance evaluation metrics are a function of the controllable coefficients in the BS and the HRIS which are the beamforming matrix $\boldsymbol{W}=[\boldsymbol{w}_1,...,\boldsymbol{w}_{K+1}]$ and the power splitting factor $\boldsymbol{\beta}$. As the HRIS-assisted MIMO DFRC system has the same controllable coefficients to determine the radar and communication performance, there is a trade-off between them. Here, we are interested in characterizing this trade-off by concurrently optimizing the joint beamforming matrix of the BS and configuring the parameters of the HRIS. To this end, we aim at maximizing the radar SINR η_r while guaranteeing communication performance Γ_c. The resulting problem can be formulated as a joint beamforming optimization problem:

$$\max_{\boldsymbol{W},\boldsymbol{\beta}} \eta_r(\boldsymbol{W},\boldsymbol{\beta};p,q), \tag{26a}$$

$$\text{s.t. } \eta_c(\boldsymbol{R},\boldsymbol{R}_k,\boldsymbol{\beta};k)\geq\Gamma_c,\ k=1,...,K, \tag{26b}$$

$$\boldsymbol{R}_i=\boldsymbol{w}_i\boldsymbol{w}_i^H,\ i=1,...,K+1, \tag{26c}$$

$$\boldsymbol{R}=\sum_{i=1}^{K+1}\boldsymbol{R}_i, \tag{26d}$$

$$0\leq\beta_l\leq 1,\ l=1,...,N, \tag{26e}$$

$$[\boldsymbol{R}]_{j,j}=P_t,\ j=1,...,T, \tag{26f}$$

where $\boldsymbol{w}_i$ is the i-th column of the $\boldsymbol{W}$, $\eta_r(\boldsymbol{W},\boldsymbol{\beta};p,q)$ and $\eta_c(\boldsymbol{R},\boldsymbol{R}_k,\boldsymbol{\beta};k)$ are defined by (24) and (15), respectively.

The objective of (26) is the radar performance of the (p,q) block detecting zone that we are interested in; (26b) is the communication constraint, with Γ_c denoting the minimum communication SINR requirement. Specifically, (26d) is defined in (14) and explains the covariance matrix $\boldsymbol{R}$ of the BS transmitted beamforming signal is the sum of sub-covariance matrices $\boldsymbol{R}_i$ of different codes. For the power constraints, (26e) denotes the power allocation of each element in the HRIS, and (26f) is the antenna power budget on the BS.

Since the optimized parameters controlling the configuration of the BS and the HRIS are coupled, the problem formulated in (26) is non-convex. Moreover, compared to [25], [26], we need to optimize the beamforming matrices of the BS and the power splitting factor $\boldsymbol{\beta}$ of the HRIS simultaneously. To address this challenging problem, we propose an efficient AO algorithm, which will be detailed in the next section.

III. Proposed Alternating Optimization Algorithm

In this section, we develop an AO algorithm to optimize the beamforming matrices of the BS and HRIS configuration parameters. We begin with introducing the HRIS optimization for fixed BS beamforming matrices in Section III-A, which we then utilize to design the BS beamforming matrices in Section III-B. The parameters update strategy during each iteration is summarized in Section III-C.

A. HRIS Configuration With Fixed BS Beamforming Matrices

In this section, we optimize the HRIS configuration with fixed BS beamforming matrix. Let $\bar{\boldsymbol{W}}^{(t)}=[\bar{\boldsymbol{W}}_c^{(t)},\bar{\boldsymbol{w}}_r^{(t)}]$ denote the fixed beamforming matrices at the BSs in the t-th iteration, with $\bar{\boldsymbol{W}}_c^{(t)}=[\bar{\boldsymbol{w}}_1^{(t)},...,\bar{\boldsymbol{w}}_K^{(t)}]$ and $\bar{\boldsymbol{w}}_r^{(t)}$ denoting the corresponding communication precoder matrix and radar beamforming vector, respectively. In this case, (26) can be simplified as

$$\begin{aligned}&\max_{\boldsymbol{\beta}}\ \eta_r(\bar{\boldsymbol{W}}^{(t)},\boldsymbol{\beta};p,q),\\ &\text{s.t. } \eta_c(\bar{\boldsymbol{R}}^{(t)},\bar{\boldsymbol{R}}_k^{(t)},\boldsymbol{\beta};k)\geq\Gamma_c,\ k=1,...,K,\\ &\quad\bar{\boldsymbol{R}}_i^{(t)}=\bar{\boldsymbol{w}}_i^{(t)}\bar{\boldsymbol{w}}_i^{(t)H},\ i=1,...,K+1,\\ &\quad\bar{\boldsymbol{R}}^{(t)}=\sum_{i=1}^{K+1}\bar{\boldsymbol{R}}_i^{(t)},\\ &\quad 0\leq\beta_l\leq 1,\ l=1,...,N,\end{aligned} \tag{27}$$

where $\bar{\boldsymbol{R}}^{(t)}$ and $\bar{\boldsymbol{R}}_i^{(t)}$ are the covariance matrix and the i-th sub-covariance matrix in the t-th iteration, respectively.

We next express $\eta_c(\bar{\boldsymbol{R}}^{(t)},\bar{\boldsymbol{R}}_k^{(t)},\boldsymbol{\beta};k)$ and $\eta_r(\bar{\boldsymbol{W}}^{(t)},\boldsymbol{\beta};p,q)$ as functions of the power splitting factor $\boldsymbol{\beta}$ in the following proposition.

Proposition 1: Given the noise variance σ^2, the channel from BS to HRIS $\boldsymbol{G}$, and the channel from the HRIS to the k-th user $\boldsymbol{h}_k$, the communication user's SINR and the radar SINR can be recast as

$$\begin{aligned}\eta_c(\boldsymbol{\beta};k)&=\frac{\boldsymbol{\beta}^T\boldsymbol{C}_3\boldsymbol{\beta}}{\hat{\boldsymbol{h}}_k^H\bar{\boldsymbol{R}}^{(t)}\hat{\boldsymbol{h}}_k-\boldsymbol{\beta}^T\boldsymbol{C}_3\boldsymbol{\beta}+\sigma^2},\ k=1,...,K,\\ \eta_r(\boldsymbol{\beta};p,q)&=\frac{(1-\boldsymbol{\beta}^T)\boldsymbol{C}_1(1-\boldsymbol{\beta})}{(1-\boldsymbol{\beta}^T)\boldsymbol{a}_r\boldsymbol{\beta}^T\boldsymbol{C}_2\boldsymbol{\beta}\boldsymbol{a}_r^H(1-\boldsymbol{\beta})+\sigma^2},\end{aligned} \tag{28}$$

where $\hat{\boldsymbol{h}}_k$ is the cascaded communication channel calculated by (9), $\boldsymbol{C}_1$, $\boldsymbol{C}_2$, $\boldsymbol{C}_3$ are Hermitian matrices defined as follows:

$$\begin{aligned}\boldsymbol{C}_1&\triangleq\left(\boldsymbol{a}_t^H\bar{\boldsymbol{w}}_r^{(t)}\bar{\boldsymbol{w}}_r^{(t)H}\boldsymbol{a}_t\right)\boldsymbol{a}_r\boldsymbol{a}_r^H,\\ \boldsymbol{C}_2&\triangleq\boldsymbol{a}_h\odot\left(\boldsymbol{G}\bar{\boldsymbol{W}}^{(t)}\right)\left(\boldsymbol{a}_h\odot\left(\boldsymbol{G}\bar{\boldsymbol{W}}^{(t)}\right)\right)^H,\\ \boldsymbol{C}_3&\triangleq\boldsymbol{h}_k\odot\left(\boldsymbol{G}\bar{\boldsymbol{w}}_k^{(t)}\right)\left(\boldsymbol{h}_k\odot\left(\boldsymbol{G}\bar{\boldsymbol{w}}_k^{(t)}\right)\right)^H,\ k=1,..,K.\end{aligned} \tag{29}$$

Here, $\bar{\boldsymbol{W}}^{(t)}=\left[\bar{\boldsymbol{w}}_1^{(t)},...,\bar{\boldsymbol{w}}_K^{(t)},\bar{\boldsymbol{w}}_r^{(t)}\right]$ is the fixed BS's beamforming matrix for communication and radar sensing, $\boldsymbol{a}_t$ is the given transmitted steering vector of radar, and $\boldsymbol{a}_h$ and $\boldsymbol{a}_r$ are the given reflection and reception steering vectors of HRIS, respectively.

Proof: See Appendix A. □

Using Proposition 1, the HRIS configuration design problem (27) can be reformulated as

$$\max_{\boldsymbol{\beta}}\frac{(1-\boldsymbol{\beta}^T)\boldsymbol{C}_1(1-\boldsymbol{\beta})}{(1-\boldsymbol{\beta}^T)\boldsymbol{a}_r\boldsymbol{\beta}^T\boldsymbol{C}_2\boldsymbol{\beta}\boldsymbol{a}_r^H(1-\boldsymbol{\beta})+\sigma^2}, \tag{30a}$$

$$\text{s.t.}\frac{\boldsymbol{\beta}^T\boldsymbol{C}_3\boldsymbol{\beta}}{\hat{\boldsymbol{h}}_k^H\bar{\boldsymbol{R}}^{(t)}\hat{\boldsymbol{h}}_k-\boldsymbol{\beta}^T\boldsymbol{C}_3\boldsymbol{\beta}+\sigma^2}\geq\Gamma_c,\ k=1,...,K, \tag{30b}$$

$$0\leq\beta_l\leq 1,\ l=1,...,N. \tag{30c}$$

Problem (30) is still non-convex and challenging to solve. To proceed, we consider the following optimization problem:

$$\min_{\boldsymbol{\beta}\in\mathcal{S}} f(\boldsymbol{\beta}) \triangleq -\eta_r(\boldsymbol{\beta};p,q)+\mathcal{R}_{\mathcal{S}}(\boldsymbol{\beta}), \tag{31}$$

where $\mathcal{S}$ represents the feasible set of the HRIS's power splitting vector $\boldsymbol{\beta}$, given by $\mathcal{S} \triangleq \{\boldsymbol{\beta}\in\mathbb{R}: 0\le\beta_l\le 1,\ l=1,...,N\}$, and $\mathcal{R}_{\mathcal{S}}(\boldsymbol{\beta})$ is a Lagrangian operator, which converts the communication constraint (30b) $\eta_c(\boldsymbol{\beta};k)\ge\Gamma_c$, for $k=1,..,K$ into the objective function. To this end, we apply the Lagrangian operator:

$$\mathcal{R}_{\mathcal{S}}(\boldsymbol{\beta}) = \lambda_1\cdot\underbrace{\alpha_1^{\Gamma_c-\eta_c(\boldsymbol{\beta};k)}}_{\triangleq g_1(\boldsymbol{\beta})}+\lambda_2\cdot\sum_{l=1}^{N}\underbrace{(2\beta_l-1)^{\alpha_2}}_{\triangleq g_2(\beta_l)}, \tag{32}$$

where λ_1 and λ_2 are strictly positive hyper-parameters to control the threshold of the communication user's SINR and manage the power of the HRIS. Formally, the communication guarantee and power constraints of the HRIS in (30) are converted into $g_1(\boldsymbol{\beta})$ and $g_2(\beta_l)$, respectively. Combining the properties of the exponential and power functions, $g_1(\boldsymbol{\beta})$ is designed as the exponential function which needs to satisfy: $0<g_1(\boldsymbol{\beta})\le 1$, when $\eta_c(\boldsymbol{\beta};k)\ge\Gamma_c,\ \forall k\in[1,K]$; $g_2(\beta_l)$ is considered as the even power function to add a high penalty to the point approaching the boundary of $\mathcal{S}$: $g_2(\beta_l)\gg 1$, when $\beta_l\notin[0,1]$. Here, we set $\alpha_1=4$ and $\alpha_2=10$ empirically.

We next propose a fast grid search (FGS) assisted auto gradient descent (AGD) algorithm to address the non-convex unconstrained optimization problem in (31). The key idea of the proposed algorithm is to utilize AD [27] to obtain a convergent solution according to the specific initialization parameters $\boldsymbol{\beta}$ generated by the proposed FGS.

We begin with the implementation of AGD, and then introduce the designed initialization strategy FGS. First, to reduce the complexity of gradient calculation, we employ the advanced AGD approach to obtain the solution of $\boldsymbol{\beta}$ after M iterations, as shown in Algorithm 1. The $(i+1)$-th iterative step in conventional gradient descent is written as:

$$\boldsymbol{\beta}^{i+1}=\boldsymbol{\beta}^{i}+\Delta_i\cdot\nabla f(\boldsymbol{\beta}^{i}), \tag{33}$$

where $\nabla(\cdot)$ is the first-order gradient operator, and Δ_i is the step size. We replace the traditional gradient operator $\nabla(\cdot)$ with the AD tool. The main concept of AD is to represent the objective function as a computational graph according to chain rules, to which the back-propagation algorithm is applied. Thus, the gradient direction at point $\boldsymbol{\beta}^i$ is given by

$$\nabla f(\boldsymbol{\beta}^{i})\approx\mathbf{BP}(f(\boldsymbol{\beta}^{i})), \tag{34}$$

where $\mathbf{BP}(\cdot)$ is the gradient computation operator based on AD and $f(\boldsymbol{\beta}^i)$ is the input objective function. Here, we use autograd of PyTorch [28] to compute $\mathbf{BP}(\cdot)$ and generate the initial $\boldsymbol{\beta}^0$ randomly. The gradient descent's step length Δ_i is substituted by the learning rate l_r and is updated by the Adam optimizer of the PyTorch [29]. Therefore, we can achieve AGD with variable step size by adjusting the learning rate.

The performance of Algorithm 1 depends heavily on the initial point $\boldsymbol{\beta}^0$. We design an FGS algorithm to find a good initial $\boldsymbol{\beta}$, as shown in Algorithm 2. The fundamental principle of FGS is to set the value corresponding to the first half entries of the vector $\boldsymbol{\beta}$ to zero:: $\boldsymbol{\beta}(1:\frac{N}{2})=\mathbf{0}_{\frac{N}{2}\times 1}$. Subsequently, the latter half of $\boldsymbol{\beta}$ is set as the unit column vector, following the multiplying of a coefficient varying in the space $\mathcal{S}$: $\boldsymbol{\beta}(\frac{N}{2}+1:N)=z\Delta_z\boldsymbol{I}_{\frac{N}{2}\times 1}$, for $z=0,...,Z_{\max}$. We define the number of grids in space $\mathcal{S}$ by $Z_{\max}$ and the grid step by Δ_z, which satisfies: $Z_{\max}\Delta_z=1$. Since the gird value $z\Delta_z$ of the slice of $\boldsymbol{\beta}$ is discrete and finite, the optimal solution of (31) is obtained by traversing all grid values in space $\mathcal{S}$. In our designed FGS algorithm, $\boldsymbol{\beta}$ is divided by $M_{\max}$ times to increase the freedom of the grid search. In the m-th iteration, we update the slice $(\zeta_1^m:\zeta_2^m)$ of the $\boldsymbol{\beta}^m$ by:

$$\begin{aligned}(\zeta_1^m:\zeta_2^m)&=\left(1:\frac{N}{2^m}\right),\\ (\zeta_1^m:\zeta_2^m)&=\left(\frac{2^m-1}{2^m}N:N\right),\end{aligned} \tag{35}$$

while holding the same search space, expressed by

$$\boldsymbol{\beta}^{m,z}(\zeta_1^m:\zeta_2^m)=z\Delta_z\boldsymbol{I}_{(\zeta_2^m-\zeta_1^m)\times 1},\ z=0,...,Z_{\max}, \tag{36}$$

Since the length of each slice needs to be not less than 1, the maximum iteration step size is $M_{\max}=\log_2^N$. Following the above discretization method, there exists an optimal solution

Algorithm 1 HRIS configuration via AGD algorithm

Input:

Initialize: $\boldsymbol{\beta}^0$, M, l_r;

for $i=0:M-1$ **do**

Calculate the objective $f(\boldsymbol{\beta}^i)=-\eta_r(\boldsymbol{\beta}^i;p,q)+\mathcal{R}_{\mathcal{S}}(\boldsymbol{\beta}^i)$;

Calculate the gradient direction $\nabla f(\boldsymbol{\beta}^i)$ according to (34);

Find the next point and update $\boldsymbol{\beta}^{i+1}=\boldsymbol{\beta}^i+l_r\cdot\nabla f(\boldsymbol{\beta}^i)$;

end for

Output:

hybrid reconfigurable intelligent surface (RIS) (HRIS) configuration vector $\boldsymbol{\beta}$.

Algorithm 2 Initialization operation via FGS algorithm

Input:

Initialize: $\boldsymbol{\beta}^0=\mathbf{0}_{N\times 1}$;

for $m=1,...,M_{\max}$ **do**

Select the update slice $(\zeta_1^m:\zeta_2^m)$ via (35);

for $z=1,...,Z_{\max}$ **do**

Grid search $\boldsymbol{\beta}^{m,z}$ according to (36);

Calculate the objective function $f(\boldsymbol{\beta}^{m,z})$;

end for

Update the next point $\boldsymbol{\beta}^{m+1}$ according to (37);

end for

Output:

HRIS initial point $\boldsymbol{\beta}^0$ used in Algorithm 1.

$\boldsymbol{\beta}^m$ piloting to the minimal value of (31). The $\boldsymbol{\beta}^m$ is thus updated based on the following operation:

$$\boldsymbol{\beta}^{m+1} = \min_{\boldsymbol{\beta}^{m,z}} f\left(\boldsymbol{\beta}^{m,z}\right),\ z = 0, ..., Z_{\max}. \tag{37}$$

In summary, we first proposed the FGS approach to obtain a good initial point $\boldsymbol{\beta}^0$, which determines the boundary of the gradient descent. Then, the AGD approach based on the back-propagation of PyTorch's autograd is applied to find a solution of (31).

B. Transmitted Beam Design With Fixed HRIS Configuration

After the HRIS configuration optimization, the power splitting vector $\bar{\boldsymbol{\beta}}^{(t)}$ of the reflected matrix $\boldsymbol{\Psi}$ and received vector $\boldsymbol{\phi}$ are obtained. We henceforth seek to optimize the joint beamforming matrix $\boldsymbol{W} = [\boldsymbol{W}_c, \boldsymbol{w}_r]$ of the BS to maximize the radar performance with the fixed HRIS configuration. The optimization problem (26) becomes:

$$\begin{aligned}
&\max_{\boldsymbol{W}} \eta_r\left(\boldsymbol{W}, \bar{\boldsymbol{\beta}}^{(t)}; p, q\right),\\
&\text{s.t. } \eta_c\left(\boldsymbol{R}, \boldsymbol{R}_k, \bar{\boldsymbol{\beta}}^{(t)}; k\right) \geq \Gamma_c,\ k = 1, ..., K,\\
&\quad \boldsymbol{R}_i = \boldsymbol{w}_i \boldsymbol{w}_i^H,\ i = 1, ..., K+1,\\
&\quad \boldsymbol{R} = \sum_{i=1}^{K+1} \boldsymbol{R}_i,\\
&\quad [\boldsymbol{R}]_{j,j} = P_t,\ j = 1, ..., T.
\end{aligned} \tag{38}$$

Similar to the expression of the user's SINR, we represent the radar's SINR in terms of the transmit sub-covariance matrices $\boldsymbol{R}_i$

$$\eta_r(\boldsymbol{R}, \boldsymbol{R}_{K+1}, \boldsymbol{\beta}; p, q) = \frac{|A_r(\boldsymbol{\beta})|^2 \boldsymbol{a}_t^H \boldsymbol{R}_{K+1} \boldsymbol{a}_t}{|A_r(\boldsymbol{\beta})|^2 \hat{\boldsymbol{a}}_h^H(\boldsymbol{\beta}) \boldsymbol{R} \hat{\boldsymbol{a}}_h(\boldsymbol{\beta}) + \sigma^2}, \tag{39}$$

where $\boldsymbol{R}_{K+1} = \boldsymbol{w}_r \boldsymbol{w}_r^H$. By updating the cascaded received scalar $\bar{A}_r^{(t)}$ and the cascaded reflected vector $\bar{\boldsymbol{a}}_h^{(t)}$ based on (21) and replacing $\boldsymbol{R}_{K+1} = \left(\boldsymbol{R} - \sum_{k=1}^K \boldsymbol{R}_k\right)$ according to (14), the SINR of the radar for a point target at position (p, q) is

$$\eta_r(\boldsymbol{R}, \boldsymbol{R}_k; p, q) = \frac{\left|\bar{A}_r^{(t)}\right|^2 \boldsymbol{a}_t^H \left(\boldsymbol{R} - \sum_{k=1}^K \boldsymbol{R}_k\right) \boldsymbol{a}_t}{\left|\bar{A}_r^{(t)}\right|^2 \bar{\boldsymbol{a}}_h^{(t)H} \boldsymbol{R} \bar{\boldsymbol{a}}_h^{(t)} + \sigma^2}. \tag{40}$$

Thus, with the respective expression of radar's SINR η_r and communication's SINR η_c in (40) and (15) in terms of $\boldsymbol{R}_i$, (38) is reformulated as

$$\begin{aligned}
&\max_{\boldsymbol{R}_1, ..., \boldsymbol{R}_K, \boldsymbol{R}_{K+1}} \eta_r(\boldsymbol{R}, \boldsymbol{R}_k; p, q),\\
&\quad \text{s.t. } \eta_c(\boldsymbol{R}, \boldsymbol{R}_k; k) \geq \Gamma_c,\ k = 1, ..., K,\\
&\quad\quad \boldsymbol{R} = \sum_{i=1}^{K+1} \boldsymbol{R}_i,\\
&\quad\quad \text{rank}(\boldsymbol{R}_i) = 1,\ i = 1, ..., K+1,\\
&\quad\quad [\boldsymbol{R}]_{j,j} = P_t,\ j = 1, ..., T.
\end{aligned} \tag{41}$$

The BS transmitted beam design problem (41) is non-convex. According to [30], (41) can be reduced to solving a sequence of convex feasibility problems. Thus, (41) is subsequently transformed as

$$\begin{aligned}
&\max_{\boldsymbol{R}_1, ..., \boldsymbol{R}_K, \boldsymbol{R}_{K+1}, \Gamma_r} \Gamma_r,\\
&\quad \text{s.t. } \eta_r(\boldsymbol{R}, \boldsymbol{R}_k; p, q) \geq \Gamma_r,\\
&\quad\quad \eta_c(\boldsymbol{R}, \boldsymbol{R}_k; k) \geq \Gamma_c,\ k = 1, ..., K,\\
&\quad\quad \boldsymbol{R} = \sum_{i=1}^{K+1} \boldsymbol{R}_i,\\
&\quad\quad \text{rank}(\boldsymbol{R}_i) = 1,\ i = 1, ..., K+1,\\
&\quad\quad [\boldsymbol{R}]_{j,j} = P_t,\ j = 1, ..., T.
\end{aligned} \tag{42}$$

Let Γ_r^* be the optimal solution of problem (42). Obviously, Γ_r^* is also the optimal value of the original problem (41). If the following feasibility problem

$$\begin{aligned}
&\text{Find } \boldsymbol{R}_1, ..., \boldsymbol{R}_K, \boldsymbol{R}_{K+1},\\
&\text{s.t. } \eta_r(\boldsymbol{R}, \boldsymbol{R}_k; p, q) \geq \Gamma_r,\\
&\quad \eta_c(\boldsymbol{R}, \boldsymbol{R}_k; k) \geq \Gamma_c,\ k = 1, ..., K,\\
&\quad \boldsymbol{R} = \sum_{i=1}^{K+1} \boldsymbol{R}_i,\\
&\quad \text{rank}(\boldsymbol{R}_i) = 1,\ i = 1, ..., K+1,\\
&\quad [\boldsymbol{R}]_{j,j} = P_t,\ j = 1, ..., T,
\end{aligned} \tag{43}$$

for a fixed Γ_r is feasible, then it follows that $\Gamma_r^* \geq \Gamma_r$. If (43) is infeasible, then $\Gamma_r^* < \Gamma_r$. Therefore, by giving a potential range of Γ_r which contains Γ_r^*, the optimal solution of (42) can be obtained via bisection search.

We next introduce the solution of (43) which is still non-convex because of the rank-one constraints. It was shown in previous works [25], [26] that (43) can be solved with SDR without loss of optimality. Omitting the rank-one constraint, (43) is relaxed to

$$\begin{aligned}
&\text{Find } \boldsymbol{R}_1, ..., \boldsymbol{R}_K, \boldsymbol{R}_{K+1}, && \text{(44a)}\\
&\text{s.t. } \eta_r(\boldsymbol{R}, \boldsymbol{R}_k; p, q) \geq \Gamma_r, && \text{(44b)}\\
&\quad \eta_c(\boldsymbol{R}, \boldsymbol{R}_k; k) \geq \Gamma_c,\ k = 1, ..., K, && \text{(44c)}\\
&\quad \boldsymbol{R} = \sum_{i=1}^{K+1} \boldsymbol{R}_i, && \text{(44d)}\\
&\quad [\boldsymbol{R}]_{j,j} = P_t,\ j = 1, ..., T. && \text{(44e)}
\end{aligned}$$

We rewrite (44b) and (44c) with the following rearrangements:

$$\Gamma_r^{-1} \boldsymbol{a}_t^H \left(\boldsymbol{R} - \sum_{k=1}^K \boldsymbol{R}_k\right) \boldsymbol{a}_t \geq \bar{\boldsymbol{a}}_h^{(t)H} \boldsymbol{R} \bar{\boldsymbol{a}}_h^{(t)} + \sigma^2 / \left|\bar{A}_r^{(t)}\right|^2, \tag{45a}$$

$$(1 + \Gamma_c^{-1}) \hat{\boldsymbol{h}}_k^{(t)H} \boldsymbol{R}_k \hat{\boldsymbol{h}}_k^{(t)} \geq \hat{\boldsymbol{h}}_k^{(t)H} \boldsymbol{R} \hat{\boldsymbol{h}}_k^{(t)} + \sigma^2,\ k = 1, ..., K, \tag{45b}$$

where the $\hat{\boldsymbol{h}}_k^{(t)}$ is the cascaded communication channel updated via (9). By respectively substituting rearrangements in (45a) and (45b) into constraints (44b) and (44c), problem (44) becomes convex and can be solved using CVX [31].

Similar to [26], the feasibility problem (44) has a closed-form solution $\hat{\boldsymbol{R}}_1, ..., \hat{\boldsymbol{R}}_K, \hat{\boldsymbol{R}}_{K+1}$, satisfying:

$$\text{rank}(\hat{\boldsymbol{R}}_i) = 1, \ i = 1, ..., K+1. \tag{46}$$

Obviously, for each Γ_r, if (44) is feasible, we have a solution that satisfies rank-one constraints in (46). By bisection search on Γ_r, we denote the solution of (44) corresponding to the maximum value of the variable Γ_r as the optimal solution of the original maximization problem (41). Then, the BS's communication beamforming matrix $\boldsymbol{W}_c = [\boldsymbol{w}_1, ..., \boldsymbol{w}_K]$ is calculated by

$$\hat{\boldsymbol{w}}_k = \left(\hat{\boldsymbol{h}}_k^{(t)H} \hat{\boldsymbol{R}}_k \hat{\boldsymbol{h}}_k^{(t)}\right)^{-\frac{1}{2}} \hat{\boldsymbol{R}}_k \hat{\boldsymbol{h}}_k^{(t)}, \ k = 1, ..., K, \tag{47}$$

and the radar beamforming vector $\hat{\boldsymbol{w}}_r$ is given by

$$\hat{\boldsymbol{w}}_r = \left(\boldsymbol{a}_t^H \left(\hat{\boldsymbol{R}} - \sum_{k=1}^{K} \hat{\boldsymbol{R}}_k\right) \boldsymbol{a}_t\right)^{-\frac{1}{2}} \left(\hat{\boldsymbol{R}} - \sum_{k=1}^{K} \hat{\boldsymbol{R}}_k\right) \boldsymbol{a}_t. \tag{48}$$

In summary, to accomplish the transmitted beam design with a fixed HRIS configuration, we convert the maximization problem (41) into a feasibility problem (42) of the variable Γ_r. For a fixed Γ_r, we solve the feasibility problem (42). By using the SDR technique [25] to relax, all the constraints in (44) are linear matrix inequalities over $\boldsymbol{R}_i$ and thus can be solved via CVX [31]. Correspondingly, the optimal value of Γ_r can be obtained by a bisection search, and the beamforming matrix $\boldsymbol{W}$ is calculated by (47) and (48).

C. Alternating Optimization Strategy in HRIS-Assisted MIMO DFRC System Beamforming

In this section, we detail how to implement the AO of the BS waveforms and HRIS beam patterns, as well as the mechanism for updating system parameters throughout this AO process in Algorithm 3.

First, as noted in solving (30), the configuration of the HRIS is determined utilizing the FGS-AGD approach. Second, we use this configuration to compute the reflected vector $\hat{\boldsymbol{a}}_h$ and received scalar A_r according to (21), which are used to address the joint transmitted beamforming design (41). Then, we use the bisection search and SDR techniques to obtain the covariance matrix $\boldsymbol{R}$ by tackling the optimization problem (41).

Note that the propagation matrices $\boldsymbol{C}_1, \boldsymbol{C}_2, \boldsymbol{C}_3$ will change with the BS beamforming matrix $\boldsymbol{W} = [\boldsymbol{W}_c, \boldsymbol{w}_r]$, so that we need to update these system parameters during iterations. Combining with the definitions of the matrices $\boldsymbol{C}_1, \boldsymbol{C}_2$, and $\boldsymbol{C}_3$, we can update these propagation matrices according to (29).

As we complete updating the HRIS-assisted MIMO DFRC system parameters, we need to optimize the HRIS configuration as well as the joint transmitted beam design of the BS continually. After several iterations, the Algorithm 3 stops when $\left|f\left(\boldsymbol{\beta}^{(t)}\right) - f\left(\boldsymbol{\beta}^{(t-1)}\right)\right| < \epsilon$.

Algorithm 3 HRIS-assisted MIMO DFRC system alternating optimization

Input:

User's SINR threshold Γ_c;
Initialization: $\boldsymbol{\beta}^0 = \boldsymbol{0}_{N\times 1}$;
Set the objective function $f(\boldsymbol{\beta})$ based on (31).

1: **repeat**
2: Compute the optimal $\boldsymbol{\beta}$ by solving the non-convex optimization problem (30) according to Algorithm 1 and Algorithm 2.
3: Calculate the reflected vector $\hat{\boldsymbol{a}}_h$ and the received scalar A_r via (21).
4: Compute the covariance matrix $\boldsymbol{R}$ and its sub-covariance matrices $\boldsymbol{R}_i$ of the BS by solving (41) with bisection search and SDR techniques.
5: Compute $\boldsymbol{w}_i$ via (47) and (48).
6: Update the matrices $\boldsymbol{C}_1, \boldsymbol{C}_2, \boldsymbol{C}_3$ via (29).
7: **until** $\left|f\left(\boldsymbol{\beta}^{(t)}\right) - f\left(\boldsymbol{\beta}^{(t-1)}\right)\right| < \epsilon$
8: Select the total beamforming matrix $\boldsymbol{W} = [\boldsymbol{w}_1, ..., \boldsymbol{w}_r]$

Output:

The HRIS configuration vector $\boldsymbol{\beta}$;
The base station (BS) beamforming matrix $\boldsymbol{W}$.

D. Complexity and Convergence Analysis

1) Computational Complexity Analysis:

- Optimization of BSs's beamforming matrices $\boldsymbol{W}_c$, $\boldsymbol{w}_r$ with fixed HRIS configuration: The semidefinite programming (SDP) problem in (44) is solved by the SDR approach during a bisection search. Specifically, given the potential values of Γ_r, the number of execution steps of the bisection search $\log_2\left(\frac{\Gamma_{r,max}-\Gamma_{r,min}}{\epsilon_1}\right)$. Similarly, given the solution accuracy ϵ_2, the complexity of using the SDR to solve (44) is $\mathcal{O}\left(T^{3.5}\log(1/\epsilon_2)\right)$[32]. Therefore, the computational complexity of BSs's beamforming algorithm is $\log_2\left(\frac{\Gamma_{r,max}-\Gamma_{r,min}}{\epsilon_1}\right) \times \mathcal{O}\left(T^{3.5}\log(1/\epsilon_2)\right)$.
- Optimization of HRIS configuration with fixed BSs beamforming matrices: Since we suggest the fast grid search assisted auto gradient descent algorithm to solve the problem in (31), the complexity of this algorithm is $M_{max}Z_{max} \times \mathcal{O}\left(MN^2\right)$, where $M_{max}Z_{max}$ is the execution times of the fast grid search, and $\mathcal{O}\left(MN^2\right)$ is the complexity of using auto gradient descent for a fixed maximum step M.

As a result, the computational complexity of the proposed alternating algorithm for each iteration is $\log_2\left(\frac{\Gamma_{r,max}-\Gamma_{r,min}}{\epsilon_1}\right) \times \mathcal{O}\left(T^{3.5}\log(1/\epsilon_2)\right) + M_{max}Z_{max} \times \mathcal{O}\left(MN^2\right)$.

2) Convergence Analysis: Algorithm 3 explains an alternating process, it is necessary to analyze the convergence of each sub-algorithm and the whole AO.

- The ascent property of the FGS-AGD: Since the FGS is a grid search-based algorithm, it obviously will converge. Next, we prove the convergence of the AGD. The objective function $f(\boldsymbol{\beta})$ is L-smooth, then AGD with the step size

$\Delta_i = 1/L$ obeys

$$f\left(\boldsymbol{\beta}^{i+1}\right) \leq f\left(\boldsymbol{\beta}^{i}\right) - \frac{1}{2L}\left\|\nabla f\left(\boldsymbol{\beta}^{i}\right)\right\|_2^2. \tag{49}$$

When the step size Δ_i is sufficiently small, AGD can guarantee a decrease in the value of the objective function $f(\boldsymbol{\beta})$. After the maximum step M, yielding

$$\begin{aligned} f\left(\boldsymbol{\beta}^{M}\right) &\leq f\left(\boldsymbol{\beta}^{0}\right) - \frac{1}{2L}\sum_{i=0}^{M-1}\left\|\nabla f\left(\boldsymbol{\beta}^{i}\right)\right\|_2^2 \\ &\leq f\left(\boldsymbol{\beta}^{0}\right) - \frac{M}{2L}\left\|\nabla f\left(\boldsymbol{\beta}^{i}\right)_{min}\right\|_2^2. \end{aligned} \tag{50}$$

Therefore, the objective function during two iterations of the AO holds that

$$f\left(\boldsymbol{W}^{t}, \boldsymbol{\beta}^{t+1}\right) \leq f\left(\boldsymbol{W}^{t}, \boldsymbol{\beta}^{t}\right) - \frac{M}{2L}\left\|\nabla f\left(\boldsymbol{W}^{t}, \boldsymbol{\beta}\right)_{min}\right\|_2^2. \tag{51}$$

The inequality in (51) verifies that the objective value in the $t+1$-th iteration is lower than the t-th iteration.

- The ascent property of the SDR with bisection search: As the goal of (41) is to maximize the radar SINR by optimizing the beamforming matrix of the BSs with the fixed $\boldsymbol{\beta}$, we have $\eta_r(\boldsymbol{W}^{t+1}, \boldsymbol{\beta}^{t+1}) \geq \eta_r(\boldsymbol{W}^{t}, \boldsymbol{\beta}^{t+1})$. However, the objective value is defined by the negative radar SINR, yielding

$$f\left(\boldsymbol{W}^{t+1}, \boldsymbol{\beta}^{t+1}\right) \leq f\left(\boldsymbol{W}^{t}, \boldsymbol{\beta}^{t+1}\right). \tag{52}$$

- The convergence of the proposed AO: In addition to the ascent property of both sub-algorithms, the convergence of the proposed AO also relies on the boundary. Combining (51) with (52), we have

$$\begin{aligned} f\left(\boldsymbol{W}^{t+1}, \boldsymbol{\beta}^{t+1}\right) \leq\ & f\left(\boldsymbol{W}^{t}, \boldsymbol{\beta}^{t}\right) \\ & - \frac{M}{2L}\left\|\nabla f\left(\boldsymbol{W}^{t}, \boldsymbol{\beta}\right)_{min}\right\|_2^2. \end{aligned} \tag{53}$$

Due to the per-antenna power constraint of the BSs in (26e) and the HRIS power limit in (26f), the radar SINR $\eta_r(\boldsymbol{W}, \boldsymbol{\beta})$ is upper-bounded so that the objective value f is lower-bounded. Consequently, the Algorithm 3 is convergent and holds:

$$\left|f\left(\boldsymbol{W}^{t+1}, \boldsymbol{\beta}^{t+1}\right) - f\left(\boldsymbol{W}^{t}, \boldsymbol{\beta}^{t}\right)\right| \leq \epsilon. \tag{54}$$

IV. Numerical Evaluations

In this section, we provide numerical results to evaluate the performance of our proposed joint beamforming design algorithm for HRIS-assisted MIMO DFRC systems. Specially, we first describe the simulation setup of the HRIS-assisted MIMO DFRC system in Section IV-A and then present some numerical results to analyze the improvements in radar and communication performance compared with the BS-only system and random-configured HRIS system in Section IV-B.

TABLE I
The DFRC Platform Simulation Configuration

Parameters	Value
Center frequency	3 GHz
The inter-element spacing in HRIS	λ
The inter-element spacing in BS	$\lambda/2$
Position of the HRIS center	$(0, 100\lambda, 30\lambda)$
Position of the BS center	$(0, 0, 300\lambda)$
Position of the user	$(75\lambda, 100\lambda, 0)$
Position of the target	$(0, 0, 0)$
Γ_c	5 dB
N	16
T	8

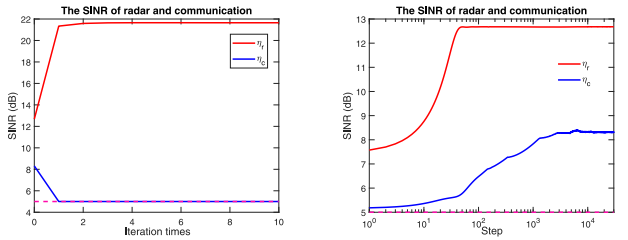

(a) Convergence of the proposed Algorithm 3.

(b) Convergence of the FGS-AGD algorithm.

Fig. 3. Convergence performance of the AO approach in Algorithm 3 and the FGS-AGD algorithm. The red line is the radar's SINR, the blue line is the communication user's SINR and the pink dash is the threshold of communication.

A. Simulation Setup

The proposed HRIS-assisted MIMO DFRC configuration is illustrated in Table. I, where the wavelength $\lambda = 0.1$ m. The total number of elements in HRIS is $N = 16$, which is a square planar array deployed on the 3D Cartesian coordinate's YOZ plane. The radar signal $s(n)$ is generated by random phase coding, and the communication symbols are generated by 16-quadrature amplitude modulation (QAM) modulation. To perform the AO approach for the formulated optimization problem, we defined the hyper-parameters in the HRIS optimization as $\lambda_1 = 4$, $\lambda_2 = 0.8$, and give the range of potential values of Γ_r as $\Gamma_{r,max} = 38$ dB, $\Gamma_{r,min} = 22$ dB.

B. Performance Analysis

First, we study the convergence performances of both the AO approach in Algorithm 3 and the FGS-AGD algorithm, where the user is deployed at $(75\lambda, 100\lambda, 0)$ and the radar target is put at 3D Cartesian coordinate center $(0, 0, 0)$. In particular, by applying the FGS-AGD for HRIS configuration optimization and the SDR technique for BS beamforming design, the convergence performance is shown in Fig. 3(a), when the per-antenna power of the BS is $P_t = 0$ dB. It indicates the proposed algorithm achieves convergence very fast in less than four iterations. In addition, the convergence of the proposed FGS-AGD method is shown in Fig. 3(b). With the assistance of the initialization operation in Algorithm 2, Algorithm 1 converges to a fixed value within 1000 iterations, which shows the efficiency and stability of the FGS-AGD algorithm.

TABLE II
THE VARIABLES AND CONFIGURATION OF EACH COMPETITOR

BS-Only	HRIS-Assisted			Profile
SDR	GA	AGD-FGS	Arbitrary selection	Algorithm
5 dB	5 dB	5 dB	5 dB	Communication Threshold
8	8	8	8	The number of BS
-	16	16	16	The number of HRIS
$\boldsymbol{W}$	$\boldsymbol{W}$, $\boldsymbol{\beta}$	$\boldsymbol{W}$, $\boldsymbol{\beta}$	$\boldsymbol{W}$	Optimized variables
P_t	P_t	P_t	P_t	Transmit power

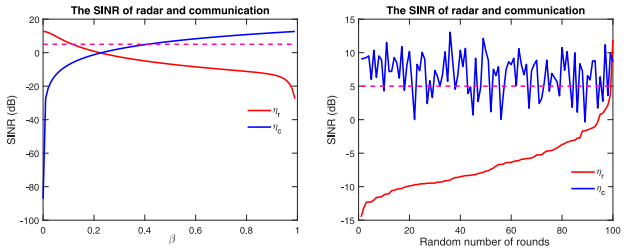

(a) Consistent. (b) Random.

Fig. 4. The SINR of radar and communication. The red line represents the SINR of radar, the blue line is the SINR of the user, and the pink dash shows the threshold of the communication (a) All elements of the HRIS have the same value. (b) The $\boldsymbol{\beta}$ is a random sequence.

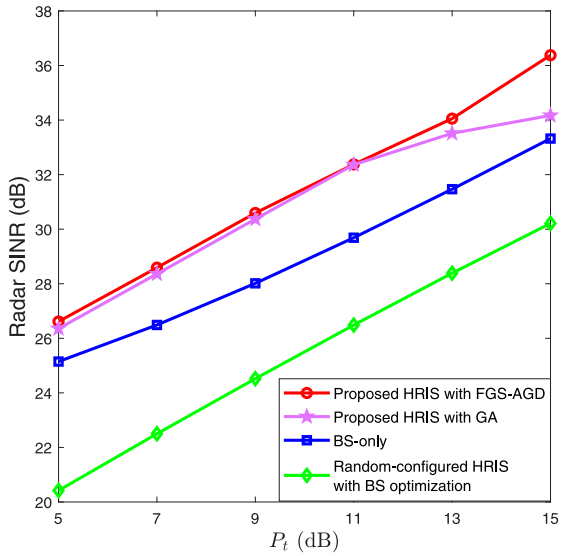

Fig. 5. Comparison of the radar SINR of three types of DFRC systems under different per-antenna power supplies.

To evaluate the effect of the HRIS configuration on the DFRC's performance, we explore the radar's and communication's SINR behaviors via different amplitude distributions on the HRIS. In Fig. 4(a), all the elements in the HRIS are set to have the same value, and the value of $\boldsymbol{\beta}$ varies between 0 and 1. It shows that the SINR of the radar will degrade when the SINR of the user tries to satisfy our constraints. Since the communication signal reflection and radar echo reception are determined by the operation of the HRIS in splitting the power of each element attached. There will be a critical trade-off between the performance of radar and communication. Fig. 4(a) verifies the essential trade-off between the SINR performance of the radar and communication. In Fig. 4(b), we randomize the value of $\boldsymbol{\beta}$, and get good performance in both radar and communication at some points. This demonstrates that the SINR performance of both radar and communication will be enhanced by HRIS configuration design.

We numerically evaluate the performance gain of our designed HRIS-assisted MIMO DFRC system with the BS-only and random-configured HRIS systems and compare the proposed FGS-AGD algorithm with a conventional optimization approach, such as genetic algorithm (GA). Specifically, the BS-only system performs both radar sensing and communication using the same hardware, and its BS has the same architecture as the proposed system. The random-configured HRIS system utilizes the HRIS to reflect or receive the arriving signals to perform communication with mobile users and radar sensing. For the algorithmic comparisons, we compare the proposed FGS-AGD with the traditional GA, and arbitrary configuration. Note that we optimize the beamforming matrix $\boldsymbol{W}$ for the BSs-only system and random-configured HRIS-assisted system. As shown in Table II, we fairly compare those four configurations in terms of the communication threshold, transmit power, the number of elements at the BS and HRIS, and the optimized variables.

In Fig. 5, compared with the BS-only and the random-configured HRIS systems, the proposed HRIS-assisted MIMO DFRC system obtains the best radar performance with the same transmit power. This demonstrates that the optimized HRIS configuration improved the performance of radar sensing while assuring the communication requirement. Moreover, the random-configured HRIS-assisted system, designed by BSs beamforming rather than alternately optimizing parameters of HRIS and BS, does not achieve its best performance. The reason for this is that the HRIS can adjust the EM environment by configuring its power splitting factor to facilitate radar sensing and communication. Then we analyze the effectiveness and robustness of the proposed algorithm. Fig. 5 shows that using the FGS-AGD algorithm can achieve better radar performance than using conventional GA for the joint problem of the BS's beamforming design and HRIS configuration, which verifies the effectiveness and robustness of the FGS-AGD.

In order to comprehend the benefit of the HRIS configuration design and the BS transmitted beam design, we provide 2D beampattern results of the HRIS by employing the proposed FGS-AGD to demonstrate the power allocation impact of the radar waveform and communication waveform of the BS. There is a concise explanation for beampattern generations of the HRIS and BSs.

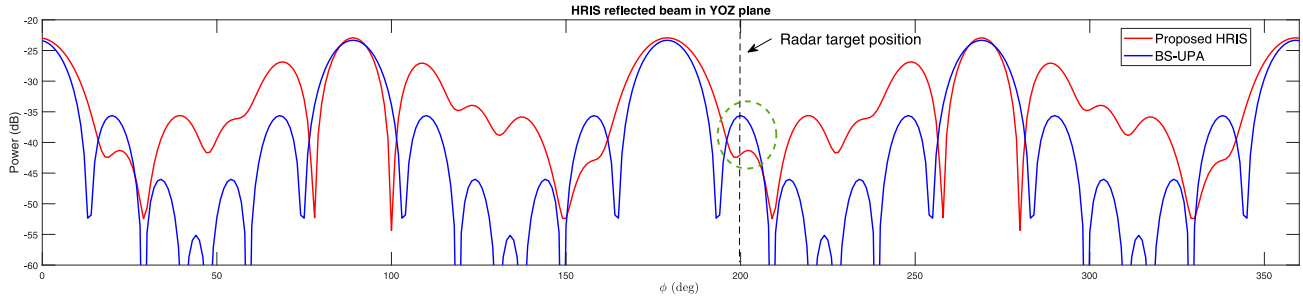

(a) Beampattern on the YOZ plane.

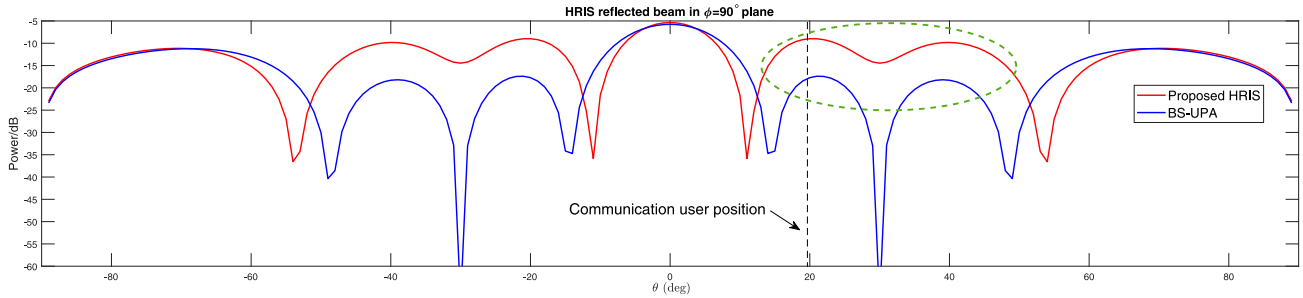

(b) Beampattern on the $\phi = 90°$ plane.

Fig. 6. The comparison of the benchmark and that designed by FGS-AGD.

- Beampattern of the HRIS: Given the configured $\boldsymbol{\beta}$, the beampattern of the HRIS is generated by

$$\begin{aligned}\mathrm{AF}(\theta,\phi) = &\sum_{m=0}^{N_x-1}\sum_{n=0}^{N_y-1} w(m,n) \\ &\exp\left(j\frac{2\pi}{\lambda}mdx\sin\theta\cos\varphi\right) \\ &\exp\left(j\frac{2\pi}{\lambda}ndy\sin\theta\sin\varphi\right), \end{aligned} \tag{55}$$

  where $w(m,n) = \beta_l$, for $m = l \bmod N_x$, $n = \lfloor l/N_x \rfloor + 1$, is the inspiring power corresponding to the value of power splitting factor $\boldsymbol{\beta}$ with the number of elements being $N_x N_y = N$.
- Beampattern of the BSs: Given the precoders of the BSs, we can define the beampatterns related to precoders of radar detection and communication as

$$\mathrm{B}_r(\theta) = \frac{\left\|\boldsymbol{a}^H(\theta)\boldsymbol{W}_r\right\|_2^2}{\mathrm{tr}(\boldsymbol{W}_r\boldsymbol{W}_r^H)}, \tag{56}$$

$$\mathrm{B}_c(\theta) = \frac{\left\|\boldsymbol{a}^H(\theta)\boldsymbol{W}_c\right\|_2^2}{\mathrm{tr}(\boldsymbol{W}_c\boldsymbol{W}_c^H)}, \tag{57}$$

  where $\boldsymbol{a}(\theta)$ is the transmit steering vector in direction θ.

To understand what we get from this HRIS configuration design, we analyze the visual results of the HRIS beampattern and investigate the effects of the radar target's location and the communication user's position on HRIS configuration design. In particular, we explore the correspondence between the beampattern direction modified by the HRIS configuration and the DFRC performance. To this aim, the beams of the HRIS radiation pattern in the YOZ plane and the $\phi = 90°$ plane are illustrated in Fig. 6(a) and 6(b), respectively. Assuming that rotation angle ϕ is formed by rotation along the y axis to the z axis, and θ is the look-down angle of the HRIS, Fig. 6 compares the beam patterns of the RIS with that the proposed HRIS designed by FGS-AGD. We observe the effect of the radar target's location on the HRIS beam design on the YOZ plane and calculate that the rotation angle ϕ of the target relative to the HRIS is around $198°$. In Fig. 6(a), the beam designed by FGS-AGD reduces the side-lobe power level at $\phi \approx 200°$, and results in the main-lobe widening, which means that the optimized HRIS configuration can reduce the interference of the HRIS reflected beam to the detection zone. Then, we study the effect of the communication user's position on the HRIS reflected beam design on the $\phi = 90°$ plane and calculate that the look-down angle of the users is around $20°$. We find a similar outcome in Fig. 6(b). The beam created by FGS-AGD increases the side-lobe power level at the look-down angle of $\theta \approx 20°$, and at the same time reduces the main lobe, which indicates that the optimized HRIS configuration increases the effective power of communication user by increasing the corresponding side-lobe power level. Hence, we infer that the HRIS adjusts the side-lobe of the beampattern by modifying the amplitude distribution of the surface components, thus increasing the quality of radar detection while maintaining the quality of communication.

Next, in the joint transmitted beam design, we employ the optimized HRIS configuration. Since we provide the FGS-AGD approach and the GA to accomplish the HRIS configuration optimization, there are two types of amplitude distributions of the HRIS. Based on each solution of HRIS beam design, we are able to calculate an optimal solution of the joint transmitted beam design. In Fig. 7, we compare the optimization results of the joint transmitted beamforming for two different HRIS amplitude distributions. By geometric calculation, the center of

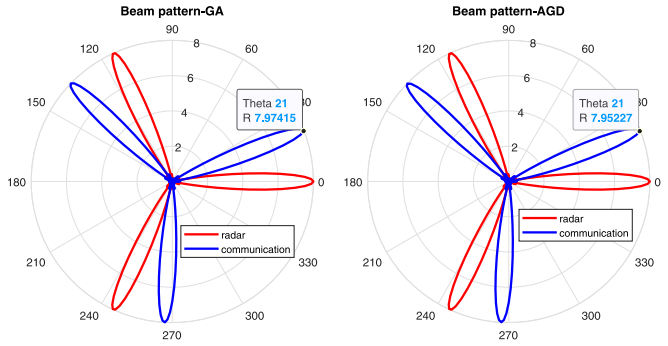

(a) GA. (b) FGS-AGD.

Fig. 7. Optimized joint transmitted beampattern. (a) shows the communication and radar waveforms of the BS by using the GA to obtain the amplitude distribution of HRIS, and (b) shows the joint transmitted waveforms by using the FGS-AGD to design the HRIS beampattern.

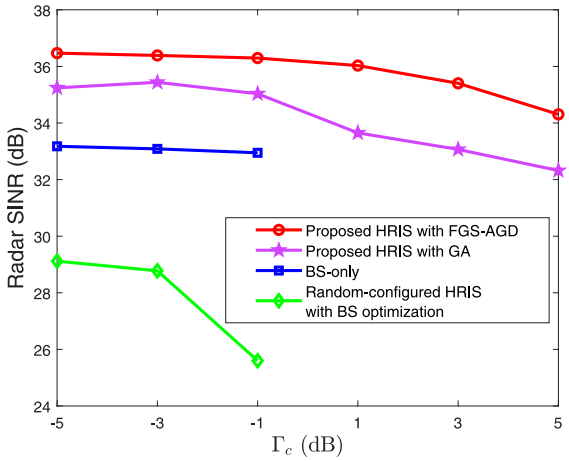

Fig. 8. Comparison of the SINR of the radar under different communication thresholds.

the HRIS is located at a position of about 20° of the look-down angle on the BS, and this angle corresponds precisely with the direction of the communication beam we designed. Meanwhile, the look-down angle of the radar beam is around 0° and points to the center of the detection zone, where our deployed radar target is placed. The fact shows that the joint beam design of the BS realizes the spatial diversity of the radar and communication waveforms and that the two beam patterns will not conflict in space.

To further evaluate the impact of spatial diversity on the performance gain of the proposed DFRC system, we explored the radar performance in a multi-user scenario. Specifically, we evaluate the radar SINR variation under different communication thresholds Γ_c in Fig. 8, considering deploying another communication user at $(150\lambda, 100\lambda, 0)$. In this scenario, the transmit power of per-antenna on the BS is set as $P_t = 15$ dB and the Γ_c varies from -5 dB to 5 dB with an increasing step set at 2 dB. From Fig. 8, we can see that with the communication threshold Γ_c rising the radar's SINR decreasing, which demonstrates a clear trade-off between radar sensing and communication. In addition, we note that the solutions of the

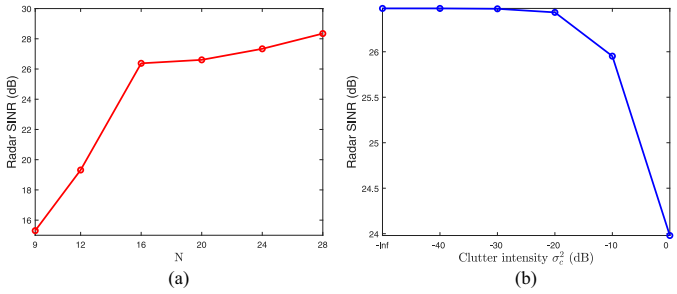

(a) (b)

Fig. 9. Radar sensing performance. (a) Radar SINR versus the number of the HRIS elements. (b) SINR for radar versus clutter intensity σ_c^2.

BS-based and random-configured HRIS-based DFRC systems disappeared when the communication threshold is over 1 dB. This phenomenon is reasonable because the second user is sheltered by the first user in the view of BS. However, our proposed system modifies the EM environment and adjusts the beam to illuminate the second user. Thus, from numerical results, our proposed HRIS-assisted DFRC system achieves the highest radar SINR than others' presented DFRC systems. Specifically, the radar's SINR improves 3 dB than the BS-only system and 6 dB over the random-configured HRIS-based system under the same communication threshold and same transmitted power.

Finally, we evaluate the impact of the number of elements in the HRIS on the radar SINR and preliminary analyze the influence on the radar performance of the cluttered environment and imperfect channel state information (CSI) of communication users.

We present the radar SINR results for different HRIS configurations under the same communication threshold $\Gamma_c = 5$ dB with the transmit power of the BS being $P_t = 5$ dB. Specifically, the number of the HRIS elements varies from 12 to 28, where the horizontal number of HRIS is fixed at 4 and the vertical number of the HRIS gradually increases. We also provide the radar performance of HRIS configuration with a square architecture, represented as $N = 9$ elements. Fig. 9(a) effectively demonstrates that the radar SINR will increase as the HRIS's elements since the HRIS is capable of managing more power for radar echo reception. However, it's worth noting that the increasing number of elements on the HRIS also leads to the high complexity of HRIS configuration optimization.

For a cluttered environment, we consider the target scene where a single target is located in the detecting zone center, and the spatial clutter is deployed at the left side of the radar target. In particular, we consider the relative clutter intensity σ_c^2, defined as

$$\sigma_c^2 = P_u / P_o \tag{58}$$

where P_u and P_o are the original clutter power and the radar target power, respectively.

Fig. 9(b) gives the radar SINR under different clutter intensity σ_c^2. Here, $\sigma_c^2 = -\infty$ dB (0) means that there is no clutter, and $\sigma_c^2 = 0$ dB means that the clutter is as strong as the radar target. It can be observed that the maximum radar SINR may degrade when σ_c^2 increases. Comparing the results for $\sigma_c^2 = -\infty$ dB (0)

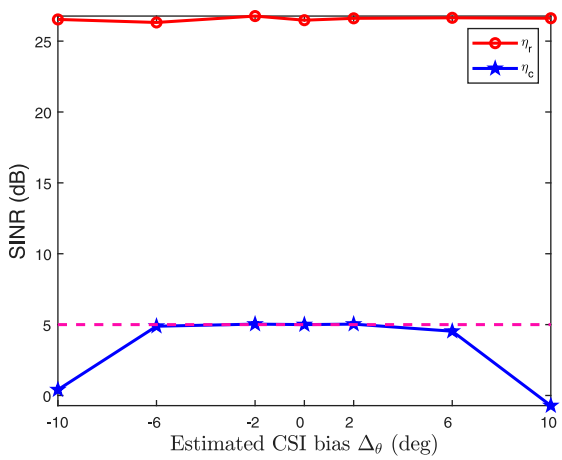

Fig. 10. SINRs for radar and communication versus imperfect CSI bias.

and $\sigma_c^2 = 0$ dB, the spatial clutter only has a minor effect on the radar sensing performance even if the relative intensity is comparable to the target. In the case of a more complex and realistic cluttered environment, the adaptation of radar beamforming to the environment is a significant topic. However, our work is only conceptual research at this stage, and in the future, we will work on the HRIS DFRC system with adaptive radar beamforming to overcome the cluttered environment.

To investigate the impact of the imperfect CSI on radar and communication SINR, we provide numerical results of the radar SINR and communication SINR with imperfect CSI under different angle bias Δ_θ. In particular, we consider the single user is deployed at $(75\lambda, 100\lambda, 0)$, the transmit power is $P_t = 5$ dB, and the communication threshold for the estimated user position is $\Gamma_c = 5$ dB. The residual error between the estimated user position and the actual user's position is defined as Δ_θ. Fig. 10 reveals that when the estimated CSI error remains below 6°, the SINR of radar detection and user communication is almost unchanged. However, as the estimated error exceeds this threshold and becomes large, the proposed system loses the capability to maintain satisfactory communication performance.

C. Discussion

1) Differences Between the Existing Hybrid RIS and Our Considered HRIS: The existing hybrid RIS architecture known as STAR-RIS has been widely considered recently [16], [17], [18]. Within the STAR-RIS framework, each antenna element of the surface splits its incoming signal power into two components. To be specific, one portion of the signal is redirected for reflection within the same region as the incident signal while the rest is transmitted. Therefore, STAR-RIS exhibits the capability of facilitating both reflection and transmission. In other words, the STAR-RIS can be viewed as a combination of the reflected-only RIS and transmitted-only RIS.

However, our considered HRIS differs from the simultaneously transmitting and reflecting (STAR)-RIS. From the perspective of hardware design, hybrid metasurfaces are designed for operating reflection and reception that allow meta-atoms to both reflect and sense [15], [20]. In our HRIS-DFRC system, each element of the surface can simultaneously reflect and receive the incoming signals. Specifically, portions of the signal are reflected to the communication user and parts of the impinging signal are received by antennas that are attached to the RF chain. We can modify these functionalities by changing the power splitting factor $\boldsymbol{\beta}$ and phase shifts.

2) Challenges in the HRIS-Assisted DFRC System: There are existing challenges associated with simultaneously transmitting radar and communication signals in an HRIS system. Firstly, the signals reflected by the HRIS have arrived at both the communication users and the radar detection zone and will interfere with both radar and communication. In this paper, we develop an AO algorithm to characterize the trade-off between the radar and communication and propose a sophisticated approach to optimize the power allocation to individual HRIS elements. This optimization strategy seeks to find a balance between radar performance and communication effectiveness in the HRIS-assisted DFRC system.

Secondly, based on the inherent characteristics of the HRIS, the RF chain is embedded in the HRIS, facilitating the radar echo reception [15], [20]. This integration increases the power efficiency of the radar system but decreases the power efficiency of the communication. Considering the hybrid metasurface configuration, the substantial number of elements on the HRIS leads to high computational complexity, which is challenging to optimize and configure. Additionally, there are significant challenges related to the high complexity of the SDR when the number of BSs is large. Some recent research explored finding more memory-efficient and computationally advantageous alternatives to solve the SDP problem [33], [34], [35]. In future work, we will consider incorporating SDR acceleration to reduce the overall complexity of the AO algorithm.

V. Conclusion

In this work, we proposed an HRIS-assisted MIMO DFRC system, where the HRIS performed reflecting communication signals and receiving radar echo concurrently. With the SINR as the evaluation metric of both radar and communication, we characterized the trade-off between radar and communication as a joint optimization problem of the BS beamforming design and the HRIS configuration design. Aiming to tackle this problem, we proposed an AO approach that consists of the FGS-AGD algorithm for solving the HRIS configuration optimization and an SDR technique for the BS's transmitted beam design. Our simulation indicated an apparent trade-off between the performance of the radar and communication while optimizing the joint design of the BS and the HRIS. Numerical results demonstrated that the HRIS-assisted system designed by the proposed approach can improve the radar sensing quality and ensure communication compared to the benchmark systems.

The fact that our work has certain underlying assumptions as the HRIS-assisted DFRC system is a theoretical concept. Firstly, we derive our model under the assumption of perfect CSI at the transmitter and the HRIS. However, in practice, this assumption may not hold with the presence of the CSI

$$\hat{\boldsymbol{h}}_k^H(\boldsymbol{\beta})\bar{\boldsymbol{R}}_k^{(t)}\hat{\boldsymbol{h}}_k(\boldsymbol{\beta}) = \boldsymbol{\beta}^T\left(\boldsymbol{h}_k \odot \left(\boldsymbol{G}\bar{\boldsymbol{w}}_k^{(t)}\right)\right)\left(\boldsymbol{h}_k \odot \left(\boldsymbol{G}\bar{\boldsymbol{w}}_k^{(t)}\right)\right)^H\boldsymbol{\beta},\ k = 1, ..., K. \tag{A.2}$$

$$\hat{\boldsymbol{a}}_h^H(\boldsymbol{\beta})\bar{\boldsymbol{W}}^{(t)}\bar{\boldsymbol{W}}^{(t)H}\hat{\boldsymbol{a}}_h(\boldsymbol{\beta}) = \boldsymbol{\beta}^T\left(\boldsymbol{a}_h \odot \left(\boldsymbol{G}\bar{\boldsymbol{W}}^{(t)}\right)\right)\left(\boldsymbol{a}_h \odot \left(\boldsymbol{G}\bar{\boldsymbol{W}}^{(t)}\right)\right)^H\boldsymbol{\beta}. \tag{A.5}$$

estimation error. In future research, the HRIS configuration and BSs beamforming design considering scenarios where only partial knowledge of the channel is available at the transmitter will be valuable to study. Secondly, in our proposed HRIS-assisted DFRC system, we proceed with radar detection in a non-cluttered environment. In more realistic scenarios, the SINR of the radar and communication degradation occurs due to clutter. In the future, we intend to investigate radar beamforming adaptations to address cluttered environments, ensuring robust performance in such scenarios.

APPENDIX

A. Proof of Proposition 1

First, we separate the reflected matrix $\boldsymbol{\Psi}(\boldsymbol{\beta})$ into power splitting factor $\boldsymbol{\beta}$: $\text{diag}([\beta_1, ..., \beta_N])$. From (9), the cascaded channel for the k-th user is given by

$$\hat{\boldsymbol{h}}_k(\boldsymbol{\beta}) = \boldsymbol{h}_k^H\text{diag}([\beta_1, ..., \beta_N])\boldsymbol{G}. \tag{A.1}$$

Next, by expressing the cascaded communication channel via (A.1) and combining with (15), the received power at the user can be recast as (A.2). Here, we denote $\boldsymbol{c}_3 = \boldsymbol{h}_k \odot \left(\boldsymbol{G}\bar{\boldsymbol{w}}_k^{(t)}\right)$ and $\boldsymbol{C}_3 = \boldsymbol{c}_3\boldsymbol{c}_3^H$. Then, the SINR at the k-th communication user in (15) is simplified to

$$\eta_c(\boldsymbol{\beta}; k) = \frac{\boldsymbol{\beta}^T\boldsymbol{C}_3\boldsymbol{\beta}}{\hat{\boldsymbol{h}}_k^H\bar{\boldsymbol{R}}^{(t)}\hat{\boldsymbol{h}}_k - \boldsymbol{\beta}^T\boldsymbol{C}_3\boldsymbol{\beta} + \sigma^2},\ k = 1, ..., K. \tag{A.3}$$

Compared to (A.2), we also transfer the expression of η_r into a combination of quadratic forms. We rewrite the cascaded reflected vector $\hat{\boldsymbol{a}}_h$ in the same way as we did in (A.1), and the decomposed expression of $\hat{\boldsymbol{a}}_h$ is

$$\hat{\boldsymbol{a}}_h^H = \boldsymbol{a}_h^H\text{diag}([\beta_1, ..., \beta_N])\boldsymbol{G}. \tag{A.4}$$

Then, combining with (A.4), the quadratic component $\hat{\boldsymbol{a}}_h^H(\boldsymbol{\beta})\bar{\boldsymbol{W}}^{(t)}\bar{\boldsymbol{W}}^{(t)H}\hat{\boldsymbol{a}}_h(\boldsymbol{\beta})$ of the interference power in (24) is rewritten by (A.5).

Next, we use $\boldsymbol{c}_2$ to replace the $\boldsymbol{a}_h \odot \left(\boldsymbol{G}\bar{\boldsymbol{W}}^{(t)}\right)$, so that the interference power from HRIS to the (p, q) block is written as

$$\mathbf{E}\left(|A_r(\boldsymbol{\beta})\hat{\boldsymbol{a}}_h^H(\boldsymbol{\beta})\boldsymbol{x}(n)|^2\right) = |A_r(\boldsymbol{\beta})|^2\boldsymbol{\beta}^T\boldsymbol{C}_2\boldsymbol{\beta}, \tag{A.6}$$

where $\boldsymbol{C}_2 = \boldsymbol{c}_2\boldsymbol{c}_2^H$ is a Hermitian matrix. Similarly, we separate the HRIS's received vector $\boldsymbol{\phi}(\boldsymbol{\beta})$ into amplitude vector $1 - \boldsymbol{\beta}$. Thus, the cascaded scalar A_r can be rewritten as

$$A_r = (1 - \boldsymbol{\beta}^T)\boldsymbol{a}_r. \tag{A.7}$$

Now, we can recast the SINR of the radar:

$$\eta_r(\boldsymbol{\beta}; p, q) = \frac{(1 - \boldsymbol{\beta}^T)\boldsymbol{a}_r\boldsymbol{a}_t^H\bar{\boldsymbol{w}}_r^{(t)}\bar{\boldsymbol{w}}_r^{(t)H}\boldsymbol{a}_t\boldsymbol{a}_r^H(1 - \boldsymbol{\beta})}{(1 - \boldsymbol{\beta}^T)\boldsymbol{a}_r\boldsymbol{\beta}^T\boldsymbol{C}_2\boldsymbol{\beta}\boldsymbol{a}_r^H(1 - \boldsymbol{\beta}) + \sigma^2}. \tag{A.8}$$

By substituting $\boldsymbol{C}_1$ for the $\left(\boldsymbol{a}_t^H\bar{\boldsymbol{w}}_r^{(t)}\bar{\boldsymbol{w}}_r^{(t)H}\boldsymbol{a}_t\right)\boldsymbol{a}_r\boldsymbol{a}_r^H$,the η_r is consequently reduced to:

$$\eta_r(\boldsymbol{\beta}; p, q) = \frac{(1 - \boldsymbol{\beta}^T)\boldsymbol{C}_1(1 - \boldsymbol{\beta})}{(1 - \boldsymbol{\beta}^T)\boldsymbol{a}_r\boldsymbol{\beta}^T\boldsymbol{C}_2\boldsymbol{\beta}\boldsymbol{a}_r^H(1 - \boldsymbol{\beta}) + \sigma^2}. \tag{A.9}$$

This concludes the proof.

REFERENCES

[1] F. Liu et al., "Integrated sensing and communications: Toward dual-functional wireless networks for 6G and beyond," *IEEE J. Sel. Areas Commun.*, vol. 40, no. 6, pp. 1728–1767, Jun. 2022.

[2] D. Ma, N. Shlezinger, T. Huang, Y. Liu, and Y. C. Eldar, "Joint radar-communication strategies for autonomous vehicles: Combining two key automotive technologies," *IEEE Signal Process. Mag.*, vol. 37, no. 4, pp. 85–97, Jul. 2020.

[3] T. Huang, N. Shlezinger, X. Xu, Y. Liu, and Y. C. Eldar, "MAJoRCom: A dual-function radar communication system using index modulation," *IEEE Trans. Signal Process.*, vol. 68, pp. 3423–3438, 2020.

[4] A. Hassanien, B. Himed, and B. D. Rigling, "A dual-function MIMO radar-communications system using frequency-hopping waveforms," in *Proc. IEEE Radar Conf. (RadarConf)*, Piscataway, NJ, USA: IEEE Press, 2017, pp. 1721–1725.

[5] R. P. Sankar, B. Deepak, and S. P. Chepuri, "Joint communication and radar sensing with reconfigurable intelligent surfaces," in *Proc. IEEE 22nd Int. Workshop Signal Process. Adv. Wireless Commun. (SPAWC)*, Piscataway, NJ, USA: IEEE Press, 2021, pp. 471–475.

[6] M. A. ElMossallamy, H. Zhang, L. Song, K. G. Seddik, Z. Han, and G. Y. Li, "Reconfigurable intelligent surfaces for wireless communications: Principles, challenges, and opportunities," *IEEE Trans. Cogn. Commun. Netw.*, vol. 6, no. 3, pp. 990–1002, Sep. 2020.

[7] Q. Wu and R. Zhang, "Towards smart and reconfigurable environment: Intelligent reflecting surface aided wireless network," *IEEE Commun. Mag.*, vol. 58, no. 1, pp. 106–112, Jan. 2020.

[8] S. P. Chepuri, N. Shlezinger, F. Liu, G. C. Alexandropoulos, S. Buzzi, and Y. C. Eldar, "Integrated sensing and communications with reconfigurable intelligent surfaces," 2022, *arXiv:2211.01003*.

[9] C. Pan et al., "Reconfigurable intelligent surfaces for 6G systems: Principles, applications, and research directions," *IEEE Commun. Mag.*, vol. 59, no. 6, pp. 14–20, Jun. 2021.

[10] A. Pitilakis et al., "A multi-functional reconfigurable metasurface: Electromagnetic design accounting for fabrication aspects," *IEEE Trans. Antennas Propag.*, vol. 69, no. 3, pp. 1440–1454, Mar. 2020.

[11] J. A. Zhang et al., "An overview of signal processing techniques for joint communication and radar sensing," *IEEE J. Sel. Topics Signal Process.*, vol. 15, no. 6, pp. 1295–1315, Nov. 2021.

[12] E. Basar, "Reconfigurable intelligent surfaces for Doppler effect and multipath fading mitigation," *Frontiers Commun. Netw.*, vol. 2, 2021, Art. no. 672857.

[13] X. Wang, Z. Fei, Z. Zheng, and J. Guo, "Joint waveform design and passive beamforming for RIS-assisted dual-functional radar-communication

system," *IEEE Trans. Veh. Technol.*, vol. 70, no. 5, pp. 5131–5136, May 2021.
[14] Z.-Q. He and X. Yuan, "Cascaded channel estimation for large intelligent metasurface assisted massive MIMO," *IEEE Wireless Commun. Lett.*, vol. 9, no. 2, pp. 210–214, Feb. 2020.
[15] G. C. Alexandropoulos, N. Shlezinger, I. Alamzadeh, M. F. Imani, H. Zhang, and Y. C. Eldar, "Hybrid reconfigurable intelligent metasurfaces: Enabling simultaneous tunable reflections and sensing for 6G wireless communications," 2021, *arXiv:2104.04690*.
[16] W. Ni, Y. Liu, Y. C. Eldar, Z. Yang, and H. Tian, "STAR-RIS integrated nonorthogonal multiple access and over-the-air federated learning: Framework, analysis, and optimization," *IEEE Internet Things J.*, vol. 9, no. 18, pp. 17136–17156, Sep. 2022.
[17] C. Wu, Y. Liu, X. Mu, X. Gu, and O. A. Dobre, "Coverage characterization of STAR-RIS networks: NOMA and OMA," *IEEE Commun. Lett.*, vol. 25, no. 9, pp. 3036–3040, Sep. 2021.
[18] M. Ahmed et al., "A survey on STAR-RIS: Use cases, recent advances, and future research challenges," *IEEE Internet Things J.*, vol. 10, no. 16, pp. 14689–14711, 2023.
[19] W. Wang, W. Ni, H. Tian, Y. C. Eldar, and R. Zhang, "Multi-functional reconfigurable intelligent surface: System modeling and performance optimization," *IEEE Trans. Wireless Commun.*, early access, Aug. 21, 2023.
[20] H. Zhang et al., "Channel estimation with hybrid reconfigurable intelligent metasurfaces," *IEEE Trans. Commun.*, vol. 71, no. 4, pp. 2441–2456, Apr. 2023.
[21] X. Zhang and H. Zhang, "Hybrid reconfigurable intelligent surfaces-assisted near-field localization," *IEEE Commun. Lett.*, vol. 27, no. 1, pp. 135–139, Jan. 2023.
[22] E. Basar, M. Di Renzo, J. De Rosny, M. Debbah, M.-S. Alouini, and R. Zhang, "Wireless communications through reconfigurable intelligent surfaces," *IEEE Access*, vol. 7, pp. 116753–116773, 2019.
[23] G. C. Alexandropoulos and E. Vlachos, "A hardware architecture for reconfigurable intelligent surfaces with minimal active elements for explicit channel estimation," in *Proc. IEEE Int. Conf. Acoust., Speech Signal Process. (ICASSP)*, Piscataway, NJ, USA: IEEE Press, 2020, pp. 9175–9179.
[24] G. C. Alexandropoulos, N. Shlezinger, I. Alamzadeh, M. F. Imani, H. Zhang, and Y. C. Eldar, "Hybrid reconfigurable intelligent metasurfaces: Enabling simultaneous tunable reflections and sensing for 6G wireless communications," *IEEE Veh. Technol. Mag.*, early access, Dec. 11, 2023.
[25] X. Liu, T. Huang, N. Shlezinger, Y. Liu, J. Zhou, and Y. C. Eldar, "Joint transmit beamforming for multiuser MIMO communications and MIMO radar," *IEEE Trans. Signal Process.*, vol. 68, pp. 3929–3944, 2020.
[26] J. Pritzker, J. Ward, and Y. C. Eldar, "Transmit precoder design approaches for dual-function radar-communication systems," 2022, *arXiv:2203.09571*.
[27] A. G. Baydin, B. A. Pearlmutter, A. A. Radul, and J. M. Siskind, "Automatic differentiation in machine learning: A survey," *J. Mach. Learn. Res.*, vol. 18, pp. 1–43, 2018.
[28] A. Paszke et al., "PyTorch: An imperative style, high-performance deep learning library," in *Proc. Adv. Neural Inf. Process. Syst.*, vol. 32, pp. 8026–8037, 2019.
[29] D. P. Kingma and J. Ba, "Adam: A method for stochastic optimization," 2014, *arXiv:1412.6980*.
[30] L. Zhang, R. Zhang, Y.-C. Liang, Y. Xin, and S. Cui, "On the relationship between the multi-antenna secrecy communications and cognitive radio communications," *IEEE Trans. Commun.*, vol. 58, no. 6, pp. 1877–1886, Jun. 2010.
[31] K.-C. Toh, M. J. Todd, and R. H. Tütüncü, "SDPT3—A MATLAB software package for semidefinite programming, version 1.3," *Optim. Methods Softw.*, vol. 11, nos. 1–4, pp. 545–581, 1999.
[32] Z.-Q. Luo, W.-K. Ma, A. M.-C. So, Y. Ye, and S. Zhang, "Semidefinite relaxation of quadratic optimization problems," *IEEE Signal Process. Mag.*, vol. 27, no. 3, pp. 20–34, 2010.
[33] J. Tranter, N. D. Sidiropoulos, X. Fu, and A. Swami, "Fast unit-modulus least squares with applications in beamforming," *IEEE Trans. Signal Process.*, vol. 65, no. 11, pp. 2875–2887, Jun. 2017.
[34] W.-G. Tang, H. Jiang, and Q. Zhang, "Range-angle decoupling and estimation for FDA-MIMO radar via atomic norm minimization and accelerated proximal gradient," *IEEE Signal Process. Lett.*, vol. 27, pp. 366–370, 2020.
[35] B. Tang, J. Tuck, and P. Stoica, "Polyphase waveform design for MIMO radar space time adaptive processing," *IEEE Trans. Signal Process.*, vol. 68, pp. 2143–2154, 2020.

Zhuoyang Liu (Graduate Student Member, IEEE) received the B.E. degree from Wuhan University, Wuhan, Hubei, China, in 2020. She is currently working toward the Ph.D. degree in electromagnetic science with the Key Laboratory of Information Science of Electromagnetic Waves, Fudan University, Shanghai, China. Her research interests include signal processing, reconfigurable intelligence surfaces, and the combination of artificial intelligence and electromagnetic waves.

Haiyang Zhang (Member, IEEE) received the B.S. degree in communication engineering from Lanzhou Jiaotong University, Lanzhou, China, in 2009, the M.S. degree in information and communication engineering from Nanjing University of Posts and Telecommunications, Nanjing, China, in 2012, and the Ph.D. degree in information and communication engineering from Southeast University, Nanjing, China, in 2017. He is currently a Professor with the School of Communications and Information Engineering, Nanjing University of Posts and Telecommunications. His research interests include 6G near-field MIMO communications, deep learning, and sampling theory.

Tianyao Huang (Member, IEEE) received the B.S. degree in telecommunication engineering from Harbin Institute of Technology, Heilongjiang, China, in 2009, and the Ph.D. degree in electronics engineering from Tsinghua University, Beijing, China, in 2014. He is currently a Professor with the School of Computer and Communication Engineering, University of Science and Technology Beijing, Beijing, P.R. China. From 2017 to 2023, he was an Assistant Professor with the Intelligence Sensing Lab, Department of Electronic Engineering, Tsinghua University. His research interests include signal processing, compressed sensing, and joint radar communications system design.

Feng Xu (Senior Member, IEEE) received the B.E. degree with honors in information engineering from the Southeast University, Nanjing, China, in 2003, and the Ph.D. degree with honors in electronic engineering from Fudan University, Shanghai, China, in 2008. He currently serves as the Vice Dean with the School of Information Science and Technology and the Director with the MoE Key Lab for Information Science of Electromagnetic Waves, Fudan University, Shanghai, China. His research interests include electromagnetic scattering theory, SAR information retrieval, and advanced radar systems.

Yonina C. Eldar (Fellow, IEEE) received the B.Sc. degree in physics and the B.Sc. degree in electrical engineering from Tel-Aviv University, Tel-Aviv, Israel, in 1995 and 1996, respectively, and the Ph.D. degree in electrical engineering and computer science from Massachusetts Institute of Technology (MIT), Cambridge, MA, USA, in 2002. She is currently a Professor with the Department of Mathematics and Computer Science, Weizmann Institute of Science, Rehovot, Israel. Her research interests include statistical signal processing, sampling theory and compressed sensing, learning and optimization methods, and their applications to biology, medical imaging and optics.